

Failure of Nielsen-Ninomiya theorem and fragile topology in two-dimensional systems with space-time inversion symmetry: application to twisted bilayer graphene at magic angle

Junyeong Ahn,^{1,2,3} Sungjoon Park,^{1,2,3} and Bohm-Jung Yang^{1,2,3,*}

¹*Department of Physics and Astronomy, Seoul National University, Seoul 08826, Korea*

²*Center for Correlated Electron Systems, Institute for Basic Science (IBS), Seoul 08826, Korea*

³*Center for Theoretical Physics (CTP), Seoul National University, Seoul 08826, Korea*

(Dated: May 26, 2022)

We show that the Wannier obstruction and the fragile topology of the nearly flat bands in twisted bilayer graphene at magic angle are manifestations of the nontrivial topology of two dimensional real wave functions characterized by the Euler class. To prove this, we examine the generic band topology of two dimensional real fermions in systems with space-time inversion I_{ST} symmetry. The Euler class is an integer topological invariant classifying real two band systems. We show that a two-band system with a nonzero Euler class cannot have I_{ST} -symmetric Wannier representation. Moreover, a two-band system with the Euler class e_2 has band crossing points whose total winding number is equal to $2e_2$. Thus the conventional Nielsen-Ninomiya theorem fails in systems with a nonzero Euler class. We propose that the topological phase transition between two insulators carrying distinct Euler classes can be described in terms of the pair creation and annihilation of vortices accompanied by winding number changes across Dirac strings. When the number of bands is bigger than two, there is a Z_2 topological invariant classifying the band topology, that is, the second Stiefel Whitney class (w_2). Two bands with an even (odd) Euler class turn into a system with $w_2 = 0$ ($w_2 = 1$) when additional trivial bands are added. Although the nontrivial second Stiefel-Whitney class remains robust against adding trivial bands, it does not impose Wannier obstruction when the number of bands is bigger than two. However, when the resulting multi-band system with the nontrivial second Stiefel-Whitney class is supplemented by additional mirror and chiral symmetries, a nontrivial second order topology and the associated corner charges are guaranteed.

I. INTRODUCTION

The recent discovery of Mott insulating states and superconductivity in twisted bilayer graphene (TBG) near the first magic angle $\theta \sim 1.05^\circ$ [1, 2] has led to a surge of research activities to understand this system [3–32]. One notable feature in the band structure of TBG is the presence of almost flat bands near charge neutrality, which are effectively decoupled from other bands by an energy gap. The reduced kinetic energy of the flat bands allows this purely carbon-based system, normally regarded as a weakly correlated system, to be an intriguing playground to examine the Mott physics and the associated unconventional superconductivity.

For a microscopic description of correlation effect in TBG, there have been several theoretical efforts to construct a tight-binding lattice model capturing the characteristic band structure of the four almost flat bands near charge neutrality [29–32]. Here we neglect the spin degrees of freedom for counting the number of bands, which is valid because the spin-orbit coupling is negligibly small. According to the low energy continuum theory which excellently describes the qualitative feature of the almost flat bands, there are two Dirac points at each K and K' point in the Moiré Brillouin zone, whose origin can be traced back to the Dirac points at each valley of the underlying graphene layers [33, 34]. The presence of massless Dirac fermions is further supported by several theoretical studies [35–38] as well as recent quantum oscillation measurement [39]. The existence of gapless Dirac points indicates the valley charge conservation $U_v(1)$ and the

space-time inversion symmetry $C_{2z}T$ where C_{2z} denotes a two-fold rotation about the z -axis and T is time-reversal symmetry [28, 29, 40]. In the presence of $U_v(1)$ and $C_{2z}T$, the four nearly flat bands are decoupled into two independent valley-filtered two-band systems, and each two-band system possesses Dirac points at K and K' . The fact that both the valley charge conservation and $C_{2z}T$ are not the exact symmetry of the TBG indicates that the symmetry of the low energy physics is larger than the exact lattice symmetry [28].

Interestingly, by putting together all the emergent symmetry including $U_v(1)$ and $C_{2z}T$, Po et al. have found an obstruction to constructing well-localized Wannier functions describing the four nearly flat bands in TBG [28, 29]. Moreover, it is shown that the obstruction originates from the fact that the two Dirac points in each valley-filtered two-band system have the same winding number, which is generally not allowed in 2D periodic systems due to the Nielsen-Ninomiya theorem [41]. In addition, based on the observation that the winding number is defined only for a two-band model in each valley, it is conjectured that the Wannier obstruction is fragile [28, 29], that is, the obstruction disappears when one considers other bands away from the Fermi energy E_F separated by an energy gap.

The main purpose of the present study is to unveil the topological nature of the nearly flat bands in TBG near a magic angle and propose a general framework to understand the band topology of 2D systems sharing the same symmetry. In particular, we show that, two bands having two Dirac points with the same winding number is endowed with an integer topological invariant, the Euler class e_2 , when the 2D spinless fermion system has space-time inversion symmetry $I_{ST} \equiv C_{2z}T$. We explicitly show that two bands having a nonzero Euler class cannot have exponentially localized Wannier representation,

* bjang@snu.ac.kr

that is, there is a Wannier obstruction. Moreover, the nonzero Euler class e_2 implies that there are band crossing points, henceforth called vortices, between the two bands, whose total winding number is equal to $2e_2$. Thus, a real two-band system carrying a nonzero e_2 evidences the violation of the Nielsen-Ninomiya theorem.

When the number of occupied bands is bigger than two, the system is characterized by another Z_2 topological invariant, that is, the second Stiefel-Whitney (SW) class w_2 . A two-band system with the Euler class e_2 turns into a multi-band system with the second Stiefel-Whitney class $w_2 = e_2 \pmod{2}$ when additional trivial bands are added. Therefore a two band system with an odd e_2 can still be characterized by the nontrivial $w_2 = 1$, which gives rise to a unit winding of the Wilson loop spectrum [42]. However, even if w_2 is nontrivial in a multi-band system, we show that there is no obstruction to constructing well-localized Wannier functions, which indicates that the band topology of a real two band system is fragile. However, when a multi-band system with $w_2 = 1$ has additional mirror and chiral symmetries, the system exhibits a higher-order band topology which guarantees the existence of corner charges.

The paper is organized as follows. We first present the topological properties of a simple four-band lattice model proposed by Zou et al. [28], which captures all the essential properties of the nearly flat bands in TBG at magic angle. After clarifying the issues related with the band topology of TBG by using the toy model, we provide a general description of the band topology of space-time (I_{ST}) symmetric spinless fermion systems in 2D. We review the concept of the Euler class in Sec. III and show that a nontrivial Euler class leads to a Wannier obstruction in Sec. III B. In Sec. IV, we prove the correspondence between the vortex winding number and the Euler class, and demonstrate the violation of Nielsen-Ninomiya theorem in real two band systems with a nonzero Euler class. Based on this correspondence, we study the transition changing the Euler class by analyzing the winding number of vortices. In section. V, we develop a new method for calculating the winding number by using the off-diagonal component of the Berry connection, which is useful for studying the pair creation and annihilation of vortices in Sec. VI. Then we show that the topological phase transition between two insulators carrying distinct Euler classes can be described via the pair creation and annihilation of vortices through the winding number reversal across a Dirac string in Sec. VII. In Sec. VIII, we describe the fragile and higher-order nature of the band topology of the nearly flat bands in twisted bilayer graphene based on the winding number annihilation and the properties of the second Stiefel-Whitney class. Finally, we conclude in Sec. IX.

II. BAND TOPOLOGY OF NEARLY FLAT BANDS IN TWISTED BILAYER GRAPHENE

Let us first clarify the issues related with the band topology of the nearly flat bands in TBG at magic angle. For this purpose, we study a simple four-band model Hamiltonian pro-

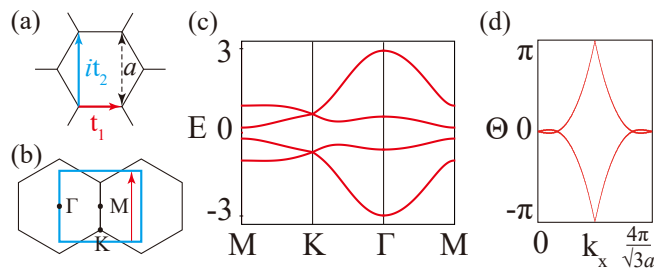


FIG. 1. (a) The definition of the hopping amplitudes $t_{1,2}$ for a four-band lattice model proposed by Zou et. al. [28]. a is the lattice constant representing the lattice vector for a Moire superlattice of TBG at magic angle. (b) High symmetry points in the Brillouin zone. $\Gamma = (0, 0)$, $M = (2\pi/\sqrt{3}a, 0)$, and $K = (2\pi/\sqrt{3}a, 2\pi/3a)$. The blue rectangle is the Brillouin zone used to compute the Wilson loop spectrum. (c) Band structure along high-symmetry lines. Both of the occupied and unoccupied bands have gapless Dirac points at K and K' . (d) Wilson loop spectrum for the lower two bands. The Wilson loop operator is calculated along the k_y direction at fixed k_x , as shown by the red arrow in (b). The unit winding of the spectrum indicates the unit Euler class $|e_2| = 1$.

posed by Zou et al. [28], which captures the essential characteristics of the nearly flat bands in TBG.

A. A four-band lattice model

The model is defined on a honeycomb lattice which represents the Moire superlattice of TBG at magic angle [28]. Putting two orbitals per site, one can construct a four-band Hamiltonian given by

$$H = \sum_{\langle ij \rangle} c_i^\dagger (\hat{t}_1)_{ij} c_j + \sum_{\langle\langle ij \rangle\rangle} c_i^\dagger s_{ij} (i\hat{t}_2)_{ij} c_j, \quad (1)$$

where $\hat{t}_1 = 0.4 + 0.6\tau_z$ and $\hat{t}_2 = 0.1\tau_x$ indicate the hopping amplitudes between the nearest-neighbor and next-nearest neighbor sites with the Pauli matrices $\tau_{x,y,z}$ representing the orbital degrees of freedom. Here we choose $s_{ij} = +1$ for $\mathbf{r}_i = \mathbf{r}_j + a\hat{y}$, which determines the rest of the s_{ij} 's because of the C_{3z} symmetry. Then the full Hamiltonian is invariant under a three-fold rotation about the z -axis C_{3z} , a two-fold rotation about the y -axis C_{2y} , and $C_{2z}T$. Namely, the lattice model has D_6 point group symmetry. This model Hamiltonian inherits the essential features of the nearly flat bands of TBG with enlarged emergent symmetries. In momentum space, the Hamiltonian becomes

$$H(\mathbf{k}) = \hat{t}_1 \left[\left(1 + 2 \cos \frac{\sqrt{3}k_x a}{2} \cos \frac{k_y a}{2} \right) \sigma_x + 2 \sin \frac{\sqrt{3}k_x a}{2} \cos \frac{k_y a}{2} \sigma_y \right] + \hat{t}_2 \left(2 \cos \frac{\sqrt{3}k_x a}{2} \sin \frac{k_y a}{2} - 2 \sin k_y a \right), \quad (2)$$

where the Pauli matrices $\sigma_{x,y,z}$ denote the sublattice degrees of freedom of the honeycomb lattice.

B. Band topology of lower two bands

The band structure of the four-band model is shown in Fig. 1(c). One can see that two lower bands are fully separated from the two upper bands. The two lower bands cross at two corners of the BZ, K and K' , forming two Dirac points with the same winding number. As pointed out in [28], the winding number of the two Dirac points can be determined by examining the mirror eigenvalues of the two occupied bands at the M point: if their mirror eigenvalues are opposite (equal), the winding numbers of the Dirac points at K and K' points are equal (opposite). In the case of the model Hamiltonian in Eq. (1), the mirror symmetry along the ΓM line can be represented by τ_z , and it can be explicitly checked that the mirror eigenvalues of the two occupied bands are indeed opposite along this line. Similarly, the two upper bands also possess two Dirac points sharing the same winding number whose winding direction is opposite to that between the lower two bands. Both the lower two bands and the upper two bands possess the same topological characteristic of the nearly flat bands of TBG in a single valley while preserving all D_6 point group symmetry [28].

Let us focus on the topological properties of the lower two bands to understand the band topology and the relevant obstruction of the nearly flat bands in TBG. One direct evidence showing the nontrivial topology of the lower two bands is the winding of the Wilson loop spectrum shown in Fig. 1(d), which is computed from the transition function in a real gauge by using the technique developed in [42]. Here the Wilson loop operator corresponds to the transition function. In the Wilson loop spectrum in Fig. 1(d), two eigenvalues change symmetrically about $\Theta = 0$ line due to the I_{ST} symmetry, and each eigenvalue winds once as k_x is varied. Below we show that the unit winding of the transition function in a real gauge indicates the unit Euler class $|e_2| = 1$, which imposes an obstruction to Wannier representation and leads to the violation of the Nielsen-Ninomiya theorem.

III. EULER CLASS AND WANNIER OBSTRUCTION FOR REAL FERMIONS IN TWO DIMENSIONS

The central symmetry governing the band topology of nearly flat bands in TBG is the space-time inversion symmetry I_{ST} . I_{ST} is an antiunitary symmetry, local in momentum space satisfying $I_{ST}^2 = +1$, so it acts like a complex conjugation in momentum space. In the absence of spin-orbit coupling, either PT or $C_{2z}T$ can be used to define I_{ST} where P indicates a spatial inversion, C_{2z} is a two-fold rotation about the z -axis, and T is time reversal symmetry. On the other hand, in the presence of spin-orbit coupling, only $C_{2z}T$ can be used to define I_{ST} since $(PT)^2 = -1$. In an I_{ST} invariant

system, we define a real gauge as

$$I_{ST}|\tilde{\psi}_{n\mathbf{k}}\rangle = |\tilde{\psi}_{n\mathbf{k}}\rangle, \quad (3)$$

where $|\tilde{\psi}_{n\mathbf{k}}\rangle$ is a Bloch state. Other possible choices of real gauges are related to each other by orthogonal transformations. This gauge condition is equivalent to $I_{ST}|\tilde{u}_{n\mathbf{k}}\rangle = |\tilde{u}_{n\mathbf{k}}\rangle$ for the cell-periodic part $|\tilde{u}_{n\mathbf{k}}\rangle = e^{-i\mathbf{k}\cdot\hat{\mathbf{r}}}|u_{n\mathbf{k}}\rangle$ since $e^{-i\mathbf{k}\cdot\hat{\mathbf{r}}}$ commutes with I_{ST} . Moreover, the transition function of $|\tilde{\psi}_{n\mathbf{k}}\rangle$ is equivalent to that of $|\tilde{u}_{n\mathbf{k}}\rangle$ if we define the periodic condition to be $|\tilde{\psi}_{n\mathbf{k}+\mathbf{G}}\rangle = |\tilde{\psi}_{n\mathbf{k}}\rangle$ and $|\tilde{u}_{n\mathbf{k}+\mathbf{G}}\rangle = e^{i\mathbf{G}\cdot\mathbf{r}}|\tilde{u}_{n\mathbf{k}}\rangle$, respectively. As is customary, we will investigate the topology of the Bloch states using the cell-periodic part. In this section, we define a topological invariant of I_{ST} symmetric two-band systems, that is, the Euler class, and explain the topological obstruction for real states arising from it.

A. The Euler class

The Euler class e_2 is an integer topological invariant for two real states which can be written as a simple flux integral form [43–45],

$$e_2 = \frac{1}{2\pi} \oint_{BZ} d\mathbf{S} \cdot \tilde{\mathbf{F}}_{12}, \quad (4)$$

where $\tilde{\mathbf{F}}_{mn}(\mathbf{k}) = \nabla_{\mathbf{k}} \times \tilde{\mathbf{A}}_{mn}(\mathbf{k})$ and $\tilde{\mathbf{A}}_{mn}(\mathbf{k}) = \langle \tilde{u}_m(\mathbf{k}) | \nabla_{\mathbf{k}} | \tilde{u}_n(\mathbf{k}) \rangle$ ($m, n = 1, 2$) are 2×2 antisymmetric real Berry curvature and connection defined by real states $|\tilde{u}_n(\mathbf{k})\rangle$ in Eq. (3). It is invariant under any $SO(2)$ gauge transformation, which has the form $O(\mathbf{k}) = \exp[i\sigma_y \phi(\mathbf{k})]$ and satisfies $\det[O(\mathbf{k})] = 1$. On the other hand, under an orientation-reversing transformation with $\det[O(\mathbf{k})] = -1$, which has the form $O(\mathbf{k}) = \sigma_z \exp[i\sigma_y \phi(\mathbf{k})]$, e_2 changes its sign. Therefore, the Euler class is well-defined only for orientable real states, that is, the states associated only with $O(\mathbf{k})$ with a unit determinant.

The flux integral form of e_2 can be connected to transition functions in the following way. To show this relation, let us notice that the 2D Brillouin zone can be deformed to a sphere when the real states are orientable along any non-contractible one-dimensional cycles as far as the topology of the real states is concerned [See Fig. 2]. Then the sphere can be divided into two hemispheres, the northern (N) and southern (S) hemispheres, which overlap along the equator. Along the equator, the real smooth wave functions $|u^N\rangle$ and $|u^S\rangle$ defined on the northern and southern hemispheres, respectively can be connected by a transition function $t^{NS} = \langle u^N | u^S \rangle = \exp[i\sigma_y \phi_{NS}] \in SO(2)$. It is straightforward to show that

$$\begin{aligned} e_2 &= \frac{1}{2\pi} \oint_{S^2} d\mathbf{S} \cdot \tilde{\mathbf{F}}_{12} \\ &= \frac{1}{2\pi} \int_N d\mathbf{S} \cdot \tilde{\mathbf{F}}_{12} + \frac{1}{2\pi} \int_S d\mathbf{S} \cdot \tilde{\mathbf{F}}_{12} \\ &= \frac{1}{2\pi} \oint_{S^1} d\mathbf{k} \cdot (\tilde{\mathbf{A}}_{N,12} - \tilde{\mathbf{A}}_{S,12}) \\ &= \frac{1}{2\pi} \oint_{S^1} d\mathbf{k} \cdot \nabla_{\mathbf{k}} \phi_{NS}, \end{aligned} \quad (5)$$

where S^1 indicates the circle along the equator. Therefore the Euler class e_2 is identical to the winding number of the transition function t^{NS} .

Let us note that Eq. (5) is also equivalent to the definition of the monopole charge [44, 46]

B. Wannier obstruction from the Euler class

Here we show that two real bands with a nontrivial Euler class suffer from an obstruction to defining exponentially localized Wannier functions respecting I_{ST} symmetry. Below, we prove the contrapositive, that the existence of exponentially localized I_{ST} -symmetric Wannier functions implies that the Euler class is trivial. Our strategy for the proof is to start from the I_{ST} -symmetric exponentially localized Wannier representation. Then, we go to the Bloch representation, find the transformation that makes $I_{ST} = K$, and finally determine whether a transition function with a nonzero winding number can arise in this real basis.

Let us recall some basic facts. Wannier states are defined to be the Fourier transform of the Bloch states:

$$|w_{n\mathbf{R}}\rangle = \frac{1}{\sqrt{N}} \sum_{\mathbf{k}} e^{-i\mathbf{k}\cdot\mathbf{R}} |\psi_{n\mathbf{k}}\rangle, \quad (6)$$

$$= \frac{1}{\sqrt{N}} \sum_{\mathbf{k}} e^{i\mathbf{k}\cdot(\hat{\mathbf{r}}-\mathbf{R})} |u_{n\mathbf{k}}\rangle. \quad (7)$$

The Bloch states $|\psi_{n\mathbf{k}}\rangle$ is given by the inverse Fourier transform, given the Wannier states. Because we assume that the Wannier functions are exponentially localized, its Bloch state is smooth over the whole Brillouin zone [47].

We first relate the I_{ST} symmetry for Wannier basis and that for Bloch basis. Since we are dealing with the case $(I_{ST})^2 = +1$, we may take

$$\langle w_{\alpha,i,-\mathbf{R}+\Delta_{\alpha\beta}} | I_{ST} | w_{\beta,j,\mathbf{R}} \rangle = \delta_{ij} \delta_{\alpha, I_{ST}\beta}, \quad (8)$$

with suitable unit cell translation $\Delta_{\alpha\beta}$. Here, α, β are Wyckoff position index and i, j are orbital index (which, in fact, we do not really need for our purpose because when I_{ST} symmetry is a site symmetry group element, its representation can be diagonalized in a spinless system). Also, $\Delta_{\alpha\beta} = -\mathbf{t}_\beta - \mathbf{t}_\alpha$ can easily be found from the action of I_{ST} symmetry in real space, $-(\mathbf{R} + \mathbf{t}_\beta) = -\mathbf{R} + \Delta_{\alpha\beta} + \mathbf{t}_\alpha$.

In the Bloch basis,

$$I_{ST} |\psi_{\beta,j,\mathbf{k}}\rangle = \frac{1}{\sqrt{N}} \sum_{\mathbf{R}} e^{-i\mathbf{k}\cdot\mathbf{R}} |w_{\alpha,j,-\mathbf{R}+\Delta_{\alpha\beta}}\rangle. \quad (9)$$

Thus, the sewing matrix is

$$\langle \psi_{\alpha,i,\mathbf{k}} | I_{ST} | \psi_{\beta,j,\mathbf{k}} \rangle = e^{-i\mathbf{k}\cdot\Delta_{\alpha\beta}} \delta_{ij} \delta_{\alpha, I_{ST}\beta}, \quad (10)$$

where the constraint $-(\mathbf{R} + \mathbf{t}_\beta) = -\mathbf{R} + \Delta_{\alpha\beta} + \mathbf{t}_\alpha$ or $\Delta_{\alpha\beta} = -\mathbf{t}_\alpha - \mathbf{t}_\beta$ is represented by $\delta_{\alpha, I_{ST}\beta}$.

If we choose a real basis $|\tilde{\psi}_{\alpha i \mathbf{k}}\rangle = U_{\alpha i, \beta j}^\dagger(\mathbf{k}) |\psi_{\beta j \mathbf{k}}\rangle$, the sewing matrix must be equal to $\delta_{\alpha\beta}$. The transformation above may not be continuous and periodic in general. Our

task now is to divide the Brillouin zone into two patches and determine whether the transition matrix for two bands resulting from two Wannier orbitals can have nontrivial winding.

The easiest case to consider is when the unit cell is left invariant under the inversion symmetry. This requires the inversion symmetry to swap the position of the two Wannier centers. Then, $I_{ST} = \sigma_x K$ in the complex basis. Under the constant unitary transformation

$$U = \frac{1}{\sqrt{2}} \begin{pmatrix} e^{-3\pi i/4} & e^{3\pi i/4} \\ e^{3\pi i/4} & e^{-3\pi i/4} \end{pmatrix}, \quad (11)$$

$I_{ST} = K$ as required. Note that there is no need to introduce patches to define a real basis.

We next consider the case when the unit cell is not left invariant under the I_{ST} symmetry, meaning that the Wannier centers occupy two different points invariant under inversion symmetry up to lattice translations. If we place the inversion center at one of the Wannier centers, the sewing matrix in the complex basis is

$$\begin{pmatrix} 1 & 0 \\ 0 & e^{-i\mathbf{k}\cdot\Delta_{\alpha\beta}} \end{pmatrix}. \quad (12)$$

We can obtain the real basis by taking

$$U = \begin{pmatrix} 1 & 0 \\ 0 & e^{i\mathbf{k}\cdot\Delta_{\alpha\beta}/2} \end{pmatrix}. \quad (13)$$

Without loss of generality, we can assume that $\Delta_{\alpha\beta} = a_{1,2}$, where $a_{1,2}$ are the two unit lattice vectors. Let us parametrize the Brillouin zone by $0 \leq k_1, k_2 < 1$, where $\mathbf{k} = k_1 \mathbf{G}_1 + k_2 \mathbf{G}_2$ and $\mathbf{G}_{1,2}$ are the reciprocal lattice vectors. Then we introduce two patches, N and S , covering $0 \leq k_1 \leq 1/2$ and $1/2 \leq k_1 \leq 1 \simeq 0$ respectively, and define $|\tilde{\psi}_{\mathbf{k}}^{N/S}\rangle = |\tilde{\psi}_{\mathbf{k}}\rangle$ for $\mathbf{k} \in N/S$. In the case of interest, the transition function is nontrivial only at $k_1 = 0$: $t^{NS}(0, k_y) = \langle \tilde{\psi}^N(0, k_2) | \tilde{\psi}^S(0, k_2) \rangle = \langle \tilde{\psi}(0, k_2) | \tilde{\psi}(1, k_2) \rangle = U^{-1}(0, k_2) U(1, k_2) = \sigma_z$, but it does not wind along the k_2 direction. In conclusion, it is not possible to realize a nontrivial Euler class in the Brillouin zone with two exponentially localized I_{ST} -symmetric Wannier functions.

IV. FAILURE OF NIELSEN-NINOMIYA THEOREM DUE TO THE EULER CLASS

In the previous section, we have shown that the Euler class is a topological invariant characterizing the Wannier obstruction for two real bands. Here we show that the Euler class is the topological invariant that explains the Wannier obstruction for nearly flat bands in TBG, which was attributed to the non-zero total winding number in the Brillouin zone. More explicitly, we show that the Euler class is equivalent to half the total winding number. To introduce some notations and set the stage for the discussion that follows, we first give a short proof of the 2D Nielsen-Ninomiya theorem, in analogy to the three-dimensional (3D) case [48]. Our main result will follow by carefully investigating the failure of the 2D Nielsen-Ninomiya theorem.

A. Two-dimensional Nielsen-Ninomiya theorem

In this section, we give a short proof of the 2D Nielsen-Ninomiya theorem that the total winding number is zero in 2D periodic systems and point out what the assumptions are. Note that we have stated this theorem by using the winding number instead of Berry phase because Berry phase is defined only modulo 2π .

Let us take two real basis states $|\tilde{u}_{1\mathbf{k}}\rangle$ and $|\tilde{u}_{2\mathbf{k}}\rangle$ such that I_{ST} is represented by the complex conjugation K (i.e., $I_{ST} = K$), so the I_{ST} symmetry condition $I_{ST}H(\mathbf{k})(I_{ST})^{-1} = H(\mathbf{k})$ requires that the matrix elements of the Hamiltonian $H_{mn}(\mathbf{k}) = \langle \tilde{u}_{m\mathbf{k}} | H(\mathbf{k}) | \tilde{u}_{n\mathbf{k}} \rangle$ to be real, that is, $H_{mn}(\mathbf{k}) = H_{mn}^*(\mathbf{k})$. Therefore,

$$H(\mathbf{k}) = r(\mathbf{k}) \cos \theta(\mathbf{k}) \sigma_1 + r(\mathbf{k}) \sin \theta(\mathbf{k}) \sigma_3 \quad (14)$$

where $r(\mathbf{k}) \geq 0$, σ_1 and σ_3 are Pauli matrices defined in the basis $\{|\tilde{u}_{1\mathbf{k}}\rangle, |\tilde{u}_{2\mathbf{k}}\rangle\}$, and a term proportional to σ_0 is ignored. Let us define a unit vector $\mathbf{n}(\mathbf{k}) = (\cos \theta(\mathbf{k}), \sin \theta(\mathbf{k}))$ away from points at which $r(\mathbf{k}) = 0$. The winding number of the Hamiltonian along a loop C is defined to be the winding number of $\mathbf{n}(\mathbf{k})$ [49]:

$$N_C = \frac{1}{2\pi} \oint_C d\mathbf{k} \cdot \nabla_{\mathbf{k}} \theta(\mathbf{k}). \quad (15)$$

Let D_i be a disk enclosing an i th vortex, so that the total winding number is given by

$$N_t = \frac{1}{2\pi} \oint_{\cup_i \partial D_i} d\mathbf{k} \cdot \nabla_{\mathbf{k}} \theta(\mathbf{k}), \quad (16)$$

where ∂D_i is the boundary of D_i . Using the Stokes' theorem, we have

$$N_t = \int_{BZ - \cup_i D_i} d\mathbf{S} \cdot \nabla_{\mathbf{k}} \times \nabla_{\mathbf{k}} \theta(\mathbf{k}) = 0 \quad (17)$$

Here, we have made an obvious assumption that the matrix elements of the two-band Hamiltonian are continuously defined throughout the Brillouin zone. This has two important implications. The first one is that when the matrix elements of the two-band Hamiltonian cannot be defined continuously in the presence of I_{ST} symmetry, a non-vanishing total winding number is allowed. We will discuss this in the following subsection. The second implication is that when the two bands are no longer isolated from the other bands, the winding number may lose its meaning. This will be discussed further in section VIA.

B. Winding number and Euler class

Let us now prove that e_2 is equal to half the total winding number of a two band Hamiltonian. We again consider the Hamiltonian in Eq. (14).

In the case when the total Berry phase, i.e. the sum of the Berry phases of the two bands, along any non-contractible 1D

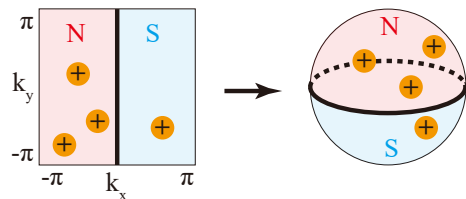


FIG. 2. Deformation of the Brillouin zone to a sphere. When the total winding number is non-zero in the Brillouin zone, Hamiltonian matrix elements are smooth only over local patches N and S , respectively. When the nontrivial transitions are restricted to $k_x = 0$ (the black bold line), the boundary of the Brillouin zone can be contracted to a point so that the Brillouin zone becomes a sphere on the right.

cycle in the Brillouin zone is trivial, we can take a spherical gauge in which we neglect the non-contractible 1D cycles and instead view the Brillouin zone as a sphere [Fig. 2]. We will discuss the case in which the Berry phase is nontrivial in Sec. VIB

One immediate consequence of the non-vanishing total winding number is that it is impossible to define a continuous Hamiltonian matrix element throughout the sphere. Thus, let us divide the sphere into N and S hemispheres such that each vortex is located in the interior of either the N or S hemisphere [Fig. 2]. On the equator, we need a transition function, $O_{NS}(\phi) \in SO(2)$, where ϕ is the azimuthal angle parametrizing the equator. The two Hamiltonian on the N and S hemispheres are connected along the equator as

$$(H_N)_{mn} = (O_{NS})_{mp} (H_S)_{pq} (O_{NS}^\dagger)_{qn} \quad (18)$$

Thus, we must have $O_{NS} = \exp(i\sigma_y(\theta_N - \theta_S)/2)$. Before moving on, note that we may assume that the two bands of our interest arise as sub-bands of a lattice Hamiltonian. Then, this transition matrix is the transition function between the two sub-bands of interest. Because the full lattice Hamiltonian is continuous, any discontinuity of the projected 2×2 Hamiltonian must originate from that of the basis states of the two subbands. Accordingly, the Euler class, which is given by the winding number of the transition function, is equal to

$$\frac{1}{4\pi} \oint_{\text{equator}} d\mathbf{k} \cdot (\nabla_{\mathbf{k}} \theta^N - \nabla_{\mathbf{k}} \theta^S) = (N_N + N_S)/2, \quad (19)$$

where $N_{N/S}$ are the sum of the winding number within N/S patch. The negative sign in the definition of N_S is there because the winding number is defined by the counterclockwise line integral with respect to the normal direction of the sphere. In conclusion, we have proved that [50]

$$e_2 = \frac{1}{2} N_t. \quad (20)$$

V. OFF-DIAGONAL BERRY PHASE

The relation in Eq. (20) allows us to study the Euler class by investigating band degeneracies which carry nontrivial winding numbers. However, it is not easy to treat the winding

number with its conventional definition, because it requires nontrivial transition functions between local patches when the total winding number in the Brillouin zone is non-zero. Instead of using the matrix element of the Hamiltonian, here we develop a new method for calculating the winding number of vortices by using energy eigenstates. We will show that the winding number of a vortex can be calculated by using an off-diagonal component of the Berry connection. Although we focus on I_{ST} -symmetric two bands here, the same method can be applied to any chiral symmetric system [See Appendix A for details]. Moreover, since the energy eigenstates can be taken smooth everywhere on the Brillouin zone except at the points of degeneracy under a smooth complex gauge, the off-diagonal Berry connection can also be smoothly defined on the punctured Brillouin zone without the need of introducing patches. Because of this reason, in this section, we relax the reality condition $I_{ST}|u_{n\mathbf{k}}\rangle = |\bar{u}_{n\mathbf{k}}\rangle$, and instead use a smooth complex gauge to define the off-diagonal Berry phase. This method will be particularly useful when we study topological phase transitions in Sec. VII.

A. Sewing matrix and Berry connection

Let $\{|u_{n\mathbf{k}}\rangle\}$ be energy eigenstates with energy $E_{n\mathbf{k}}$. In this basis, the sewing matrix G of the I_{ST} operator is defined by

$$G_{mn}(\mathbf{k}) = \langle u_{m\mathbf{k}} | I_{ST} | u_{n\mathbf{k}} \rangle. \quad (21)$$

This sewing matrix is diagonal when the energy eigenstates are non-degenerate, because I_{ST} operator does not change the energy of the state when it is a symmetry operator. Then

$$G(\mathbf{k}) = \begin{pmatrix} e^{i\theta_1(\mathbf{k})} & 0 \\ 0 & e^{i\theta_2(\mathbf{k})} \end{pmatrix}. \quad (22)$$

Equation (21) can be used to show that the Berry connection

$$A_{mn}(\mathbf{k}) = \langle u_{m\mathbf{k}} | \nabla_{\mathbf{k}} | u_{n\mathbf{k}} \rangle, \quad (23)$$

in I_{ST} -symmetric systems satisfies

$$\mathbf{A}(\mathbf{k}) = G(\mathbf{k})\mathbf{A}^*(\mathbf{k})G^{-1}(\mathbf{k}) + G(\mathbf{k})\nabla_{\mathbf{k}}G^{-1}(\mathbf{k}). \quad (24)$$

In a two-band system, or more generally for two subbands of a larger system, the constraint equation can be exactly solved on the non-degenerate region. We have

$$\mathbf{A}(\mathbf{k}) = \begin{pmatrix} -\frac{i}{2}\nabla_{\mathbf{k}}\theta_1(\mathbf{k}) & \mathbf{a}(\mathbf{k})e^{i\chi(\mathbf{k})} \\ -\mathbf{a}(\mathbf{k})e^{-i\chi(\mathbf{k})} & -\frac{i}{2}\nabla_{\mathbf{k}}\theta_2(\mathbf{k}) \end{pmatrix}, \quad (25)$$

where $\chi(\mathbf{k}) = (\theta_1(\mathbf{k}) - \theta_2(\mathbf{k}))/2$, and we defined $\mathbf{a}(\mathbf{k}) = e^{-i\chi(\mathbf{k})}\mathbf{A}_{12}(\mathbf{k})$, which is the only real parameter undetermined by the sewing matrix. Here $\chi(\mathbf{k})$ is defined modulo π because $\theta_1(\mathbf{k})$ and $\theta_2(\mathbf{k})$ are defined modulo 2π . Correspondingly, a definite global sign of $\mathbf{a}(\mathbf{k})$ is fixed after choosing the global phase of $e^{i\chi(\mathbf{k})}$.

Let us emphasize that $\mathbf{a}(\mathbf{k})$ is the gauge-invariant part of the off-diagonal Berry connection $\mathbf{A}_{12}(\mathbf{k})$: it is invariant under

diagonal gauge transformations, which do not mix different energy eigenstates. Under a gauge transformation

$$|u_{n\mathbf{k}}\rangle \rightarrow |u'_{n\mathbf{k}}\rangle = e^{i\zeta_n(\mathbf{k})}|u_{n\mathbf{k}}\rangle, \quad (26)$$

where $n = 1, 2$, we have $\theta'_n(\mathbf{k}) = \theta_n(\mathbf{k}) - 2\zeta_n(\mathbf{k})$, and $\mathbf{A}'_{12}(\mathbf{k}) = e^{-i(\zeta_1(\mathbf{k}) - \zeta_2(\mathbf{k}))}\mathbf{A}_{12}(\mathbf{k})$. Then

$$\mathbf{a}'(\mathbf{k}) = \mathbf{A}'_{12}(\mathbf{k})e^{-i\chi'(\mathbf{k})} = \mathbf{A}_{12}(\mathbf{k})e^{-i\chi(\mathbf{k})} = \mathbf{a}(\mathbf{k}). \quad (27)$$

B. Winding number from off-diagonal Berry connection

Now we show that $\mathbf{a}(\mathbf{k})$ contains the full information on the winding number. Let us consider the following eigenstates of the two-band Hamiltonian in Eq. (14).

$$|u_{1\mathbf{k}}\rangle = \begin{pmatrix} \sin \phi(\mathbf{k}) \\ \cos \phi(\mathbf{k}) \end{pmatrix}, \quad |u_{2\mathbf{k}}\rangle = \begin{pmatrix} -\cos \phi(\mathbf{k}) \\ \sin \phi(\mathbf{k}) \end{pmatrix}, \quad (28)$$

where $\phi(\mathbf{k}) = \theta(\mathbf{k})/2 - \pi/4$. In this choice of gauge, $G(\mathbf{k}) = 1$, and the Berry connection is given by

$$\mathbf{A}(\mathbf{k}) = \begin{pmatrix} 0 & \frac{1}{2}\nabla_{\mathbf{k}}\theta(\mathbf{k}) \\ -\frac{1}{2}\nabla_{\mathbf{k}}\theta(\mathbf{k}) & 0 \end{pmatrix}. \quad (29)$$

From this expression, we get $\mathbf{a}(\mathbf{k}) = \frac{1}{2}\nabla_{\mathbf{k}}\theta(\mathbf{k})$, such that

$$\oint_{S^1} d\mathbf{k} \cdot \mathbf{a}(\mathbf{k}) = \frac{1}{2} \oint_{S^1} d\mathbf{k} \cdot \nabla_{\mathbf{k}}\theta(\mathbf{k}) = N_{S^1}\pi. \quad (30)$$

Since $\mathbf{a}(\mathbf{k})$ is invariant under any diagonal gauge transformations, the *off-diagonal Berry phase* defined by $\oint_{S^1} d\mathbf{k} \cdot \mathbf{a}(\mathbf{k})$ in any smooth energy eigenstate basis gives the desired winding number N_{S^1} .

When we consider two subbands of a larger system, the off-diagonal Berry phase can still capture the winding number of vortices although it is not quantized in general. As one can see from $\nabla_{\mathbf{k}} \times \mathbf{a}(\mathbf{k}) = \tilde{F}_{12} \neq 0$ in a real eigenstate basis, $\oint_{S^1} d\mathbf{k} \cdot \mathbf{a}(\mathbf{k})$ is not quantized. However, the above relation between the off-diagonal Berry phase and the winding number in Eq. (30) is still valid in the vicinity of a vortex, where the other bands except the two bands of our interest contribute to the off-diagonal Berry phase negligibly. In other words, as a disk D containing a vortex v shrinks to the vortex site, we have

$$\oint_{\partial D \rightarrow v} d\mathbf{k} \cdot \mathbf{a}(\mathbf{k}) = N(v)\pi, \quad (31)$$

where $N(v)$ is the winding number of a vortex v . This is consistent with the correspondence between the Euler class and the winding number we derived above. Consider a punctured sphere $S^2_p \equiv S^2 - \sum_i D_i$, where D_i is an infinitesimal disk on the sphere containing a vortex v_i . Then, in the limit of vanishing D_i , we find

$$\begin{aligned} e_2 &= \frac{1}{2\pi} \oint_{S^2_p} d\mathbf{S} \cdot \nabla_{\mathbf{k}} \times \mathbf{a}(\mathbf{k}) \\ &= \frac{1}{2\pi} \sum_i \oint_{\partial D_i} d\mathbf{k} \cdot \mathbf{a}(\mathbf{k}) \\ &= \frac{1}{2} N_t. \end{aligned} \quad (32)$$

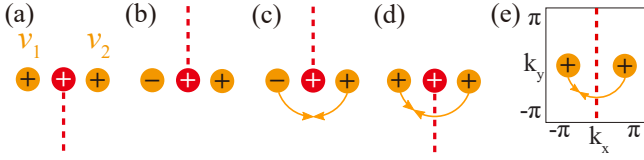


FIG. 3. Pair annihilation process in a 2D Brillouin zone. (a) v_1 and v_2 are the vortices between bands 1 and 2. They are indicated by orange dots with the + or - representing their winding number. The red dot indicates a π Berry flux generator, which can be thought of as a vortex between bands 2 and 3. The Dirac string is represented by the red dashed line. (b) An alternative choice of the Dirac string. (c) The vortices can only be annihilated by moving downwards. (d) A vortex reverses its winding number when it crosses a Dirac string. Thus, the vortices can be annihilated as shown. (e) Pair annihilation of two vortices with the same winding number in a Brillouin zone. A Dirac string along the k_y direction indicates the non-trivial Berry phase along the k_x direction, which allows the pair annihilation of the two vortices.

VI. PAIR ANNIHILATION OF VORTICES

In this section, we discuss how a pair annihilation of vortices can occur. In the previous sections, we have described how a non-zero Euler class gives a non-zero total winding number, and how the winding number can be defined in terms of the off-diagonal Berry connection. A crucial assumption for achieving a non-zero total winding number was that the total Berry phase along any non-contractible cycle must be zero.

To study the effect of non-zero Berry phase, let us notice that it is impossible to consistently choose a definite global sign of $\mathbf{a}(\mathbf{k})$ when the total Berry phase is nontrivial along a loop. Suppose we take a smooth and periodic gauge around a loop C parametrized by $0 \leq k < 2\pi$. Then, the sewing matrix and the Berry connection are also smooth and periodic along the cycle. The periodic condition $G(2\pi) = G(0)$ gives

$$\begin{aligned} e^{i\chi(2\pi)} &= e^{i(\theta_1(2\pi) - \theta_1(0) + \theta_2(2\pi) - \theta_2(0)) / 2} e^{i\chi(0)} \\ &= e^{-\oint_C d\mathbf{k} \cdot \text{Tr} \mathbf{A}} e^{i\chi(0)}. \end{aligned} \quad (33)$$

Since $\mathbf{A}(2\pi) = \mathbf{A}(0)$, we find that

$$\mathbf{a}(2\pi) = e^{\oint_C d\mathbf{k} \cdot \text{Tr} \mathbf{A}} \mathbf{a}(0). \quad (34)$$

Thus, we cannot assign the global sign of $\mathbf{a}(\mathbf{k})$ unambiguously when the total Berry phase is nontrivial. This implies that a pair creation of two vortices with the same winding number can occur when the band gap closes and the nontrivial Berry phase is generated by gap-closing points. In this section, we describe this mechanism of the pair creation and annihilation of vortices. We also comment on the case with nontrivial Berry phase along the non-contractible 1D cycles in the Brillouin zone.

A. Pair annihilation process

In Fig. 3 (a), we show a schematic picture of a part of the 2D Brillouin zone. The orange dots labeled by v_1 and v_2 represent

two vortices between energy bands 1 and 2, which are the bands we are interested in. Let us assume that v_1 and v_2 have the same winding number. We will describe how v_1 and v_2 can be pair-annihilated when the band gap between these two bands and another band (band 3) closes to form additional gap closing points (Dirac points). Notice that in the viewpoint of bands 1 and 2, such an additional gap closing point acts as a π Berry phase generator in the sense that the sum of the Berry phases for bands 1 and 2 calculated around a loop enclosing the additional gap closing point formed by bands 1 or 2 and the band 3 is π . Such a π Berry phase generator is shown as a red dot in Fig. 3.

According to Eq. (34), $\mathbf{a}(\mathbf{k})$ changes sign when it circles around the red dot once, because of the π Berry phase. For the purpose of discussing the winding number of vortices, we must therefore introduce a branch cut, shown as a dashed line in Fig. 3 (a). Across this branch cut, the sign of both $\mathbf{a}(\mathbf{k})$ and $e^{i\chi(\mathbf{k})}$ changes, so that \mathbf{A}_{12} is well defined. We will refer to this branch cut as a *Dirac string*, in analogy to the Dirac string that arises from three-dimensional magnetic monopoles [51]. As in the three-dimensional case, this Dirac string also ends when it reaches another π Berry flux generator because the total Berry phase surrounding the two π Berry flux generator is 2π so that the factor $e^{i\chi(\mathbf{k})}$ is well defined around any curve surrounding them.

To illustrate the most important property of the Dirac string, suppose that v_1 and v_2 have the same winding number with the choice of Dirac string in Fig. 3(a). Then, consider a process in which the Dirac string rotates clockwise to the configuration shown in Fig. 3 (b). This is equivalent to changing the sign of $\mathbf{a}(\mathbf{k})$ at the points where the Dirac string swaps by, so that the winding number of v_1 also changes. One implication of this result is that v_1 and v_2 can be annihilated only by circling around the red dot downwards, as shown in Fig. 3 (c). Also, by considering the reverse process in which the Dirac string is fixed and the vortices move, one sees that *whenever a vortex crosses a Dirac string, its winding number changes its sign*. Thus, if we consider the annihilation process shown in Fig. 3 (d), the winding number of the vortex v_2 changes the sign upon crossing the Dirac string, before v_1 and v_2 are pair annihilated.

B. Instability of vortices in non-orientable cases

Up to now, we have dealt with the case when the Euler class is well defined by assuming that the total Berry phase along any non-contractible cycle in the Brillouin zone is trivial. However, when there is a nontrivial Berry phase along any non-contractible 1D cycle on the Brillouin zone torus, and thus the Euler class is ill-defined, two vortices with the same winding number can be pair annihilated even when band 1 and 2 are well separated from other bands. The reason why two vortices can be pair-annihilated is basically the same as the previous case discussed in section VI A. Namely, the nontrivial Berry phase along a nontrivial cycle implies that there must be a closed Dirac string along the other non-contractible 1D cycle of the Brillouin zone torus. Because the winding num-

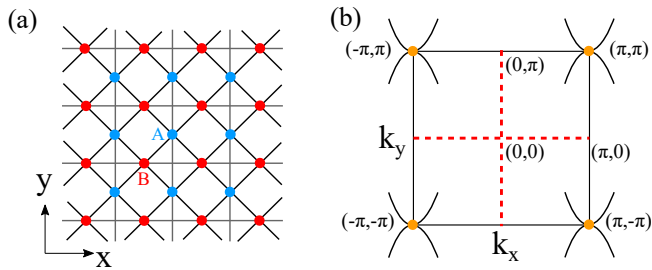


FIG. 4. Quadratic band crossing model introduced by Sun et. al.,[52]. (a) The structure of the checkerboard lattice with two sites in a unit cell where the blue (red) dot represents A (B) sublattice site. (b) Low energy band structure in the Brillouin zone. The orange dot at $M = (\pi, \pi)$ represents a quadratic band crossing with the winding number ± 2 . A red dotted line indicates a Dirac string across which the winding number of a band crossing point changes the sign.

ber of a vortex changes whenever it crosses a Dirac string, even if two vortices have the same winding number at the beginning, after transporting one of the vortices across the Dirac string, two vortices can be pair-annihilated as shown in Fig. 3 (e).

For instance, let us consider the two-band lattice model on checkerboard lattice proposed in [52], which falls exactly into this category. As explained below, this model contains a single quadratic band crossing point (QBCP) with the winding number ± 2 at $M = (\pi, \pi)$ in the BZ. The presence of a well-defined tight-binding Hamiltonian indicates that there is no Wannier obstruction for the two bands, and thus the Euler class of this model should be zero. Naively, the presence of the band crossing point with the winding number two seems to be incompatible with the fact that the Euler class of the system is trivial. One way to reconcile this contradiction is to consider nontrivial Berry phase along non-contractible cycles of the BZ. Below we show that this is indeed the case, that is, the total winding number is ill-defined due to the π Berry phase along non-contractible cycles of the BZ.

The checkerboard lattice is shown in Fig. 4(a). The relevant tight binding Hamiltonian with one orbital per lattice site is

$$H = - \sum_{ij} t_{ij} c_i^\dagger c_j, \quad (35)$$

where $t_{ij} = t$ for nearest neighbor sites, $t_{ij} = t'(t'')$ for next nearest neighbor sites connected (not connected) by vertical or horizontal bonds. This spinless model has time reversal T symmetry and four-fold rotation C_{4z} symmetry about the center of the smallest square formed by A (blue) and B (red) sites. Since the system has $C_{2z}T = (C_{4z})^2T$ symmetry, the theoretical idea developed in the preceding sections can be directly applied.

After Fourier transformation taking into account the atomic positions within the unit cell, we obtain

$$H(\mathbf{k}) = d_0(\mathbf{k})\sigma_0 + d_x(\mathbf{k})\sigma_x + d_z(\mathbf{k})\sigma_z, \quad (36)$$

where $d_0(\mathbf{k}) = -(t' + t'')(\cos k_x + \cos k_y)$, $d_x(\mathbf{k}) = -4t \cos \frac{k_x}{2} \cos \frac{k_y}{2}$, and $d_z(\mathbf{k}) = -(t' - t'')(\cos k_y - \cos k_x)$.

It is important to note that this Hamiltonian is real but not periodic. In contrast, if we take the Fourier transformation with respect to the position of the unit cell neglecting the atomic positions in the unit cell, $d_0(\mathbf{k})$ and $d_z(\mathbf{k})$ remain the same, but we now have $d_x(\mathbf{k}) - id_y(\mathbf{k}) = -(1 + e^{-ik_x} + e^{-ik_y} + e^{-i(k_x+k_y)})$. Thus, the Hamiltonian is complex and periodic in this case.

If we choose the real basis in which the winding number is well-defined and expand the Hamiltonian near the M point, we obtain $d_x = -tk_xk_y$ and $d_z = \frac{(t'-t'')}{2}(k_x^2 - k_y^2)$ so that the winding number is ± 2 where the sign depends on the choice of the parameters. We find $H(\mathbf{k} + \mathbf{G}_i) = \sigma_z H(\mathbf{k}) \sigma_z$, where \mathbf{G}_i is the reciprocal lattice vector either along the k_x or k_y direction. This indicates that the Hamiltonian is discontinuous at the BZ boundary. Since $\det(\sigma_z) = -1$, an orientation reversing transformation is necessary to glue the Hamiltonian matrix elements at the BZ boundary.

This non-orientability indicates that the total Berry phase along the k_x and k_y directions should be π , which can be explicitly checked by computing the Berry phase using a complex smooth basis.

As shown in Sec. VI A, the π -Berry phase along both the k_x and k_y directions indicates the presence of Dirac strings along the two non-contractible cycles of the Brillouin zone. [See Fig. 4(b).] If the C_{4z} symmetry is broken while C_{2z} is preserved, the QBCP can be split into two Dirac points and be annihilated when they merge at $X = (\pi, 0)$ or $Y = (0, \pi)$ after crossing a Dirac string. This phenomenon is indeed observed in a related tight binding model on the checkerboard lattice in [53].

Let us note that the appearance of the Dirac string is related to the absence of a C_{2z} -invariant unit cell. If we Fourier transform a tight-binding Hamiltonian, we have $H(\mathbf{k} + \mathbf{G}) = V^{-1}(\mathbf{G})H(\mathbf{k})V(\mathbf{G})$ in general, where $V_{\alpha\beta}(\mathbf{k}) = \exp(i\mathbf{k} \cdot \mathbf{r}_\alpha) \delta_{\alpha\beta}$, and α, β are indices labelling the atomic sites. When $\det V = -1$, an odd number of atoms are displaced by a half lattice vector from a C_{2z} center, so we cannot take a C_{2z} -invariant unit cell.

VII. TOPOLOGICAL PHASE TRANSITION

In this section, we describe the topological phase transition between insulators with different Euler classes. Since the Euler class is well-defined for two-band systems, we consider the insulators with two occupied bands. We first discuss the transition between 2D insulators with $e_2 = 1$ and $e_2 = 0$, respectively. Then, we provide an alternative description for the same process in terms of monopole nodal lines in three dimensions (3D). Finally, we consider spinful systems with $C_{2z}T$ symmetry and describe the transition between a quantum spin Hall insulator and a normal insulator. Here we show how the total vorticity in the Brillouin zone can be related with the Fu-Kane-Mele (FKM) invariant [54].

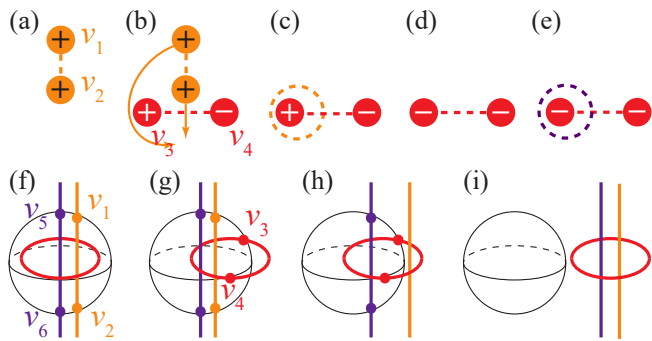


FIG. 5. Topological phase transition from $e_2 = 1$ to $e_2 = 0$ by a pair annihilation of vortices. (a) v_1 and v_2 are the vortices formed by two occupied bands (bands 1 and 2). The orange dashed line is the Dirac string of v_1 and v_2 in the viewpoint of bands 2 and 3 where band 3 is the lowest energy unoccupied band. (b) v_3 and v_4 are vortices that form when the band gap between the occupied (bands 1, 2) and unoccupied band (band 3) closes. The red dashed line is the Dirac string between v_3 and v_4 as seen by bands 1 and 2. v_1 and v_2 can be annihilated as shown, because v_2 changes its winding number when it crosses the red dashed line. (c) Annihilation of v_1 and v_2 leaves behind a Dirac string as shown. (d) Due to the Dirac string left behind in (c), the winding number of v_3 changes. (e) It may seem that v_3 and v_4 cannot annihilate, but this is not the case because processes similar to those shown in (a)~(c) occur in the unoccupied bands to leave another loop of a Dirac string (purple), which also changes the winding number of v_3 . (f)~(i) The same process in the point of view of monopole lines in three dimensions (3D). The orange (purple) line is the band crossing points between occupied (unoccupied) bands. The red line is the band crossing points between bands 2 and 3. The sphere can be thought of as the Brillouin zone in (a)~(e).

A. Pair annihilation of vortices

In this section, we describe how a topological phase transition from a $e_2 = 1$ phase to a $e_2 = 0$ phase can occur. For a minimal description, we consider a four-band system at half-filling, where the occupied bands (band 1,2) have $e_2 = 1$, and the unoccupied bands (band 3,4) have $e_2 = -1$ as in the case shown in Fig. 1. Recalling that an insulator with $|e_2| = 1$ has a pair of vortices with the same winding number, we must either annihilate the two vortices or create another pair of vortices with the opposite winding number so that the total winding number of bands 1 and 2 becomes zero. For simplicity, we discuss only the former case, shown in Fig. 5 (a)~(e).

Following the convention in the previous section, the pair of vortices between bands 1 and 2 with the same winding numbers are labeled by v_1 and v_2 , as shown in Fig. 5 (a). For the phase transition to occur, a pair of vortices with opposite winding number (v_3 and v_4) must be formed between bands 2 and 3 via a band gap closing, as shown in Fig. 5(b). Notice that we have drawn two Dirac strings for each of the pairs, because in the viewpoint of bands 1 and 2, v_3 and v_4 act as π Berry flux generators, while in the viewpoint of bands 2 and 3, v_1 and v_2 act as π Berry flux generators. Thus, v_1 and v_2 can be annihilated by passing through the Dirac string, as shown in Fig. 5 (b) and (c). However, this leaves behind a ring of the Dirac string, as shown in Fig. 5 (c), so that v_3 and v_4 even-

tually has the same winding number as in Fig. 5 (d) after v_3 crosses the ring of the Dirac string which shrinks to a point and disappears in the end. However, we have only focused on bands 1, 2, and 3, but we must not forget about the vortices between bands 3 and 4. When the vortices in bands 3 and 4 go through a similar annihilation process, another Dirac string forming a ring will be left as in Fig. 5 (c). This will in turn change the winding number of v_3 or v_4 in Fig. 5 (d). Thus, v_3 and v_4 can be annihilated to open up the band gap, resulting in a trivial insulator.

B. Alternative description in terms of a monopole nodal line

It is possible to give this pair annihilation process an alternative description in terms of a nodal line with a monopole charge in 3D. For this, let us consider again the four-band model with two occupied bands (bands 1, 2) and two unoccupied bands (bands 3, 4), which are now in 3D space. Moreover, let us suppose that the band crossing between bands 2 and 3 forms a monopole nodal line at E_F . One immediate physical consequence arising from the monopole charge of the nodal line is that another nodal line formed between bands 1 and 2 should be linked with the monopole nodal line as shown in [42]. Because of this linking structure, a sphere wrapping the monopole nodal line should cross the other nodal line below E_F at two points as shown in Fig. 5 (f). Considering the wrapping sphere as a 2D BZ, the crossing between the sphere and the nodal line below E_F indicates the Dirac points formed between two occupied bands. Since the monopole charge is identical to the Euler class when the number of occupied bands is two [42], the wrapping sphere exactly corresponds to a 2D insulator with $e_2 = 1$ having two vortices with the same winding number between the two occupied bands. Note that in Fig. 5 (f), we have also drawn a purple line next to the orange line, to indicate that the gap closing points formed by the unoccupied bands (bands 3 and 4), for which the same comments apply as those for the occupied bands. Also, the points at which the orange (purple) line crosses the sphere corresponds to the vortices between bands 1 and 2 (bands 3 and 4) in the 2D insulator. Then, we see that for the occupied bands to become trivial, the orange line and the purple line should leave the sphere before the red loop does. The trajectories of the crossing points between the sphere and the three nodal lines (orange, red, purple) correspond to the process shown in Fig. 5 (a-d).

C. Topological phase transition in the presence of spin-orbit coupling

Up to now, we have focused on the case without spin orbit coupling. Even in the presence of spin-orbit coupling, however, $I_{ST} = C_{2z}T$ acts like a complex conjugation satisfying $(C_{2z}T)^2 = +1$, so it can protect vortices in the absence of inversion P symmetry. In a recent work [40], it was shown that pair creation and pair annihilation of Dirac points can mediate a topological phase transition between a

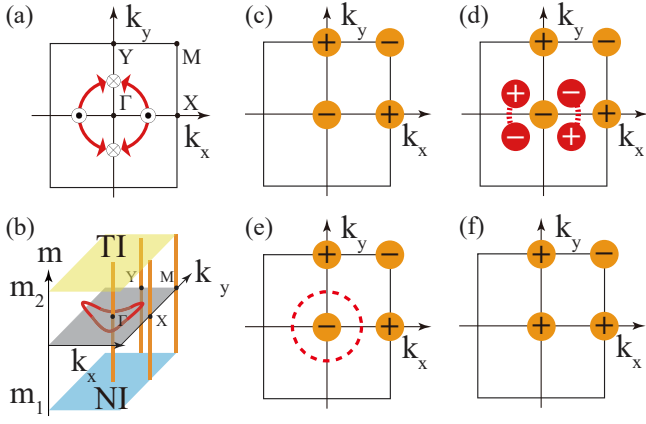


FIG. 6. Topological phase transition between a normal insulator (NI) and a quantum spin Hall insulator (TI) in spin-orbit coupled noncentrosymmetric systems with C_{2z} and T symmetries. (a) Trajectory of Dirac points (or vortices) in the intermediate gapless phase. (b) A nodal line, representing the trajectory of Dirac points in the 3D space (k_x, k_y, m) where m denotes a tuning parameter. The nodal line (red) encircles the Kramers degenerate lines (orange) an odd number of times. (c-f) Change of the winding number of the Kramers degenerate points above and below the Fermi energy E_F . The vortices of Dirac points at E_F and Kramers degenerate points are shown in red and orange, respectively. The \pm sign shows the local winding number of vortices. Dashed lines in (d) and (e) are Dirac strings across which the winding number of a Kramers degenerate point changes its sign. The total winding number of Kramers degenerate points below E_F (and also above E_F) changes from zero in (c) to two in (f).

normal insulator and a quantum spin Hall insulator in spin-orbit coupled noncentrosymmetric systems with T and C_{2z} symmetries. In the course of a topological phase transition, the trajectory of Dirac points form a closed loop surrounding time-reversal-invariant momenta (TRIM) an odd number of times as shown in Fig. 6(a). This pair creation and pair annihilation processes can also be understood in terms of the winding number changes across a Dirac string as described below. Such an alternative description is possible due to the equivalence between the second Stiefel-Whitney class and the Fu-Kane-Mele invariant in the system as explained in detail in Appendix B.

For convenience, let us suppose that the system is composed of two occupied bands and two unoccupied bands, although the topological phase transition is well-defined when the number of bands is larger. Because of time reversal symmetry, occupied bands are always degenerate at TRIM. Then in the 3D space (k_x, k_y, m) including a tuning parameter m controlling the phase transition, the Kramers degeneracies form four straight nodal lines along the m -direction as shown in Fig. 6 (b). If a normal insulator with $e_2 = 0$ and a topological insulator with $e_2 = 1$ exist for $m < m_1$ and $m = m_2 > m_1$, respectively, the trajectory of Dirac points corresponds to the intersection between the red nodal line and the constant m planes in Fig. 6 (b) as m is tuned in the range $m_1 < m < m_2$. Due to the straight nodal lines from Kramers degeneracies, any nodal loop, representing the trajectory of Dirac points, centered at a TRIM should be a monopole line

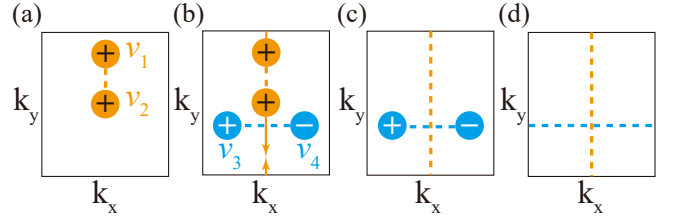


FIG. 7. Fragility of vortices in a two-band system (bands 1, 2) with $e_2 = 1$ against adding one trivial band (band 0) below the Fermi energy. The added trivial band is assumed to have the lowest energy level. The box represents the 2D Brillouin zone. (a) Vortices v_1 and v_2 with the same winding number formed between band 1 and band 2. The dashed orange line is the Dirac string for vortices which may be formed between band 0 and band 1. (b) Pair annihilation of v_1 and v_2 after a band inversion between band 0 and band 1. Blue vortices v_3 and v_4 are pair-created after the band inversion between bands 0 and 1. v_1 and v_2 can be pair-annihilated because the winding number of v_2 changes the sign after it crosses the blue Dirac string. (c) The orange Dirac string extends along a non-contractible cycle after v_1 and v_2 are pair-annihilated. (d) The blue Dirac string also winds a non-contractible 1D cycle after v_3 and v_4 are pair-annihilated.

due to the linking structure [42]. Then, the shape of the trajectory of Dirac points reflects the correspondence between the closed trajectory of vortices and the relevant change of the topological invariant.

Explicitly, let us explain how the winding number transition is related to the closed trajectory of gap-closing points. Consider a transition from a normal insulator with $e_2 = 0$ to a quantum spin Hall insulator with $e_2 = 1$, and assume, for simplicity, that the band structure of the normal insulator has no degeneracy other than the Kramers degeneracy. Then, $e_2 = 0$ indicates that the total winding number of the Kramers degenerate points below the Fermi energy E_F should be zero as shown in Fig. 6(c). When the band gap closes and vortices are pair-created at the momentum \mathbf{k} and $-\mathbf{k}$, Dirac strings connecting each pair of vortices are also generated [Fig.6(d)]. Let us note that both C_{2z} and T require that the winding number of vortices at \mathbf{k} and $-\mathbf{k}$ is equal. As the Dirac strings follow the trajectory of the vortices, they eventually form a closed loop around a TRIM after the pair annihilation of vortices [Fig. 6(e)]. Then, the Dirac string can be removed after flipping the sign of the winding number of the Kramers degenerate point encircling [Fig. 6(f)]. Because of the sign change, the total winding number of Kramers degenerate points becomes two. This indicates the change of the topological invariant e_2 from zero to one.

VIII. FRAGILE TOPOLOGY AND HIGHER-ORDER TOPOLOGY

In Ref. [29], Po et al. have conjectured that the topological characteristic of two bands having two vortices with the identical winding number is fragile [55], based on the observation that the integer winding number of the vortices is defined only for two bands. Our theory is consistent with this conjecture in

that the Euler class is also defined only for two bands. However, there is a caveat. Although the Euler class is defined only for two bands, its parity remains meaningful even when the number of bands becomes larger than two due to the additional trivial bands. In fact, the Euler class modulo two is identical to another Z_2 topological invariant, known as second Stiefel-Whitney class w_2 , that is well-defined for any number of bands. Namely, if the Euler class of the two-band model is even (odd), w_2 of the system should remain zero (one) after the inclusion of additional trivial bands [42]. Here we show that the nontrivial second Stiefel-Whitney class ($w_2 = 1$) does not induce a Wannier obstruction when the number of bands is bigger than two. However, this does not mean that an insulator with the nontrivial w_2 , dubbed a Stiefel-Whitney insulator [42], is featureless. As shown in [56], anomalous corner states can exist in Stiefel-Whitney insulators, which can be stabilized when additional mirror and chiral symmetries are present. We show that the corner charges are induced by the configuration of the Wannier centers constrained by the non-trivial second Stiefel-Whitney class. Therefore the band topology of the nearly flat bands in TBG carrying unit Euler class is fragile but exhibits the second-order topology due to the nontrivial second Stiefel-Whitney class.

A. Reduction of winding numbers from Z to Z_2

Let us first clarify the meaning that the winding number of a vortex reduces from Z to Z_2 when the number of bands is increased from two to more than two. The reduction is due to the ambiguity in the sign of the winding number in the presence of a Dirac string, which was introduced before. We show that this puts a global constraint on the pair creation and annihilation processes of vortices.

For instance, let us consider a two-band system (band 1 and band 2) with two vortices v_1 and v_2 with the same winding number. One can add a trivial band (band 0) below the band minimum of the two band system. When a band inversion happens between band 0 and band 1, two new vortices v_3 and v_4 with the opposite winding numbers can be created. Between v_3 and v_4 , a Dirac string exists across which the winding number of v_1 or v_2 changes its sign. Then, v_1 and v_2 can be pair-annihilated after one of them crosses the Dirac string. If the pair annihilation occurs across the Brillouin zone boundary as shown in Fig. 7(c,d), v_3 and v_4 also can be annihilated across the other Brillouin zone boundary. Thus, eventually, each band is decoupled from other bands without any band crossing inbetween. The pair annihilation of v_1 and v_2 , which had the same winding number in the absence of band 0, indicates that the integer winding number is not well-defined anymore after the addition of band 0. A quantized Berry phase, which is a Z_2 invariant, would be the only remaining invariant assigned to each vortex.

Interestingly, such pair annihilations of two pairs of vortices leave behind two Dirac strings, each encircling a non-contractible cycle in the Brillouin zone. Let us note that the torus geometry of the Brillouin zone is essential to complete this process. The appearance of two orthogonal closed Dirac

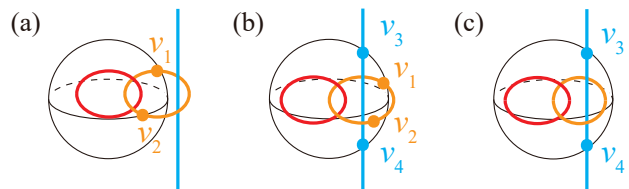


FIG. 8. Robustness of vortices on a sphere against adding a trivial band. The blue, orange, and red lines are formed between band 0 and band 1, between band 1 and band 2, and between band 2 and band 3, respectively. (a) Vortices v_1 and v_2 with the same winding number. (b) Pair creation of v_3 and v_4 . v_1 and v_2 can be pair-annihilated after crossing the Dirac string existing between vortices v_3 and v_4 . (c) After the pair annihilation of v_1 and v_2 . The resulting v_3 and v_4 have the same winding number.

strings indicates that the bands 0, 1, 2 acquire nontrivial Berry phases along the k_x and k_y cycles, Φ_x and Φ_y such that bands 0, 1, and 2 have $(\Phi_x, \Phi_y) = (0, \pi)$, (π, π) , and $(\pi, 0)$, respectively, after the completion of the pair annihilation process.

In contrast, let us remark that the above process cannot occur if the Brillouin zone has a spherical geometry. Since all loops are contractible on a sphere, Berry phase should always be trivial. On a sphere, a pair annihilation of vortices with the same winding number formed between bands 1 and 2 necessarily lead to a pair creation of other vortices with the same winding number between another pair of bands, (for instance, between bands 0 and 1) as shown in Fig. 5 (a-d). This is related to the robust linking structure of monopole nodal lines in the 3D Brillouin zone as illustrated in Fig. 8.

B. Absence of Wannier obstruction

As for the Wannier obstruction, let us note that each decoupled band after pair annihilation of vortices is Wannier representable since a single isolated band with zero Chern number always has a Wannier representation [57]. In fact, the Wannier representation is allowed even if the vortices v_1 and v_2 exist after the addition of the trivial band 0. This is because the corresponding transition functions can be diagonalized after a suitable gauge transformation, which mixes energy eigenstates at each \mathbf{k} in general, while keeping the Hamiltonian intact.

Let us note that the Wannier centers for three bands 0, 1, 2 are uniquely determined here. Since the Berry phase for bands 0, 1, and 2 are $(\Phi_1, \Phi_2) = (0, \pi)$, (π, π) , and $(\pi, 0)$, respectively, the relevant Wannier centers are given by $(0, a_2/2)$, $(a_1/2, a_2/2)$, and $(a_1/2, 0)$, because $\frac{1}{2\pi}(a_1\Phi_1, a_2\Phi_2)$ corresponds to the Wannier center, where $a_{i=1,2}$ are lattice constants. This can be shown as follows. Let us recall that the Wannier center of the n th band is related to a Berry connection by

$$\mathbf{W}_n = \langle n\mathbf{0} | \hat{\mathbf{r}} | n\mathbf{0} \rangle = V_{\text{cell}} \int_{\text{BZ}} \frac{d^2k}{(2\pi)^2} \mathbf{A}_n, \quad (37)$$

where V_{cell} is the volume of the unit cell, and $|n\mathbf{R}\rangle$ is the

Wannier state of the n th band \mathcal{B}_n . Then, because of the quantization of the Berry phase,

$$\begin{aligned} (\mathbf{W}_n)_i &= V_{\text{cell}} \int \frac{dk_{\perp}}{2\pi} \left(\int \frac{dk_i}{2\pi} (\mathbf{A}_n)_i \right) \\ &= V_{\text{cell}} \int \frac{dk_{\perp}}{2\pi} \left(\frac{\Phi_i(\mathcal{B}_n)}{2\pi} \right) = \frac{a_i}{2} \frac{\Phi_i(\mathcal{B}_n)}{\pi}. \end{aligned} \quad (38)$$

Let us note that although the three bands have a Wannier representation, the second Stiefel-Whitney class is still non-trivial. This fact can be confirmed by using the Whitney sum formula [42, 43] for the second Stiefel-Whitney class in the following way. When all the bands are non-degenerate, the second Stiefel-Whitney class of the whole bands $\mathcal{B} \equiv \oplus_n \mathcal{B}_n$ ($n = 0, 1, 2$) satisfies

$$w_2(\mathcal{B}) = \frac{1}{\pi^2} \sum_{n \neq m} \Phi_1(\mathcal{B}_n) \Phi_2(\mathcal{B}_m) = 4 \sum_{n \neq m} (\mathbf{W}_n)_1 (\mathbf{W}_m)_2. \quad (39)$$

From the Berry phases for bands 0, 1, 2, given by $(\Phi_1, \Phi_2) = (0, \pi)$, (π, π) , and $(\pi, 0)$, one can easily find $w_2 = 1$.

C. Second-order topology characterized by nontrivial second Stiefel-Whitney class

Even though $w_2 = 1$ states are Wannier representable, it does not mean that there is no physical consequence associated with them. Let us note that w_2 in Eq. (39) has the form of the electric quadrupole moment [59–61] as pointed out in [42]:

$$\begin{aligned} &4 \sum_{n \neq m} (\mathbf{W}_n)_1 (\mathbf{W}_m)_2 \\ &= 4 \sum_{n, m} (\mathbf{W}_n)_1 (\mathbf{W}_m)_2 - 4 \sum_n (\mathbf{W}_n)_1 (\mathbf{W}_n)_2, \\ &= 4 \sum_n (\mathbf{W}_n)_1 (\mathbf{W}_n)_2 \pmod{2}, \end{aligned} \quad (40)$$

where $\sum_n (\mathbf{W}_n)_1 = \sum_n (\mathbf{W}_n)_2 = 0$. In fact, anomalous corner states can be induced in systems with $w_2 = 1$ as shown in [56].

The presence of corner charges can be understood as follows. Suppose that a two-dimensional system is composed of two quantum Hall insulators with Chern numbers $c = 1$ and $c = -1$, respectively, which are related to each other by I_{ST} [Fig. 9(a)]. This system is a Stiefel-Whitney insulator with $w_2 = 1$, which can be confirmed by the winding pattern of the Wilson loop spectrum. For example, the Wilson loop spectrum in Fig. 1(d) is composed of two spectral flows, one going upward and the other going downward, each of which corresponds to $c = 1$ and $c = -1$, respectively. In this particular limit of the Stiefel-Whitney insulator, two counter-propagating chiral edge states exist [Fig. 9(a)]. After I_{ST} -preserving mass terms are added to the boundary, the chiral edge states can be gapped, but mirror symmetry forces the mass term to vanish at the mirror-invariant corners on the

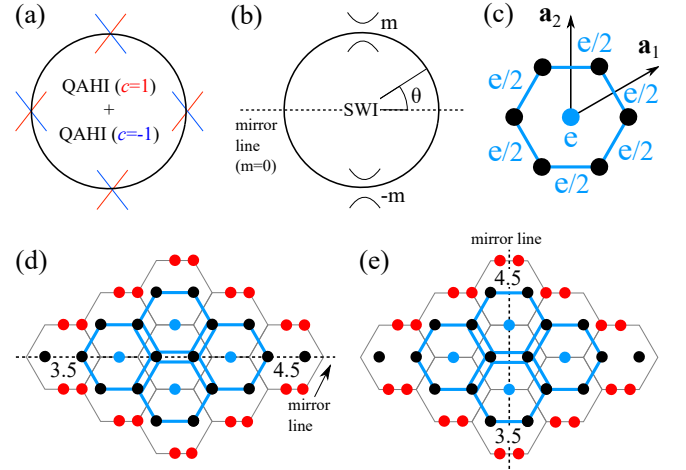


FIG. 9. Corner states in Stiefel-Whitney insulators. (a) A system composed of two copies of quantum Hall insulators with two counter-propagating edge states, which can be considered as a particular example of Stiefel-Whitney insulators. (b) A Stiefel-Whitney insulator with additional mirror M and chiral S symmetries. A mass term $m(\theta)$ compatible with $C_{2z}T$, M , and S symmetries can open a gap at the edge. M requires the mass term to change the sign at the mirror-invariant corners. (c) The distribution of the Wannier centers for four electrons around a hexagon. Black dots indicate the atomic sites. A blue dot (link) denotes an electric (a half electric) charge localized. (d,e) A schematic figure describing the charge distribution for a finite-size Stiefel-Whitney insulator on the honeycomb lattice with (d) $M_y : y \rightarrow -y$ and (e) $M_x : x \rightarrow -x$ symmetries, respectively. Red dots (blue dots and links) represent electric charges localized at the edge (in the bulk). For charge counting, when a dot or a link is shared by n unit cells, we assume that each involved unit cell takes $1/n$ -th of the relevant localized charge. Here the honeycomb lattice with black dots indicates the finite-size lattice structure whereas the gray honeycomb lattice underneath describes an array of the hexagonal unit cells, each of which contains two black dots in the middle. The number 3.5 and 4.5 shows the number of localized electrons or the integrated probability density in the unit cell at the mirror-invariant corners. In both cases (d) and (f), half corner charges are accumulated or depleted at mirror-invariant corners. $C_{2z}T$ symmetry is broken due to the requirement that a corner state is localized at one corner, similar to the case in Su-Schrieffer-Heeger model [58–60].

edge. To see this, let us consider a disk geometry with the radius R shown in Fig. 9(b) for simplicity. When chiral operation S is represented by $S = \sigma_z$, the edge Hamiltonian is given by $H_{\text{edge}}(\theta) = -i(v/R)\sigma_y \partial_\theta + m(\theta)\sigma_x$, where θ denotes the polar angle and v indicates the tangential velocity along the boundary [62, 63]. Then, the mirror operator M is uniquely determined to be $M = \sigma_z$ by the condition that it commutes S and satisfies the mirror symmetry condition $MH_{\text{edge}}(\theta)M^{-1} = H_{\text{edge}}(-\theta)$. Since the mirror symmetry imposes $m(-\theta) = -m(\theta)$, the mass vanishes at the mirror invariant corners with $\theta = 0$ and $\theta = \pi$.

Let us note that, although the role of mirror and chiral symmetries is not explicitly explained in [56], the presence of these two symmetries, which are actually very slightly broken, is the origin of the corner states found in [56] [See Ap-

pendix C].

Alternatively, we can understand the origin of the anomalous corner charges in terms of localized Wannier centers when the number of occupied bands is bigger than two. For convenience, let us consider a hexagonal lattice with four electrons per unit cell. Suppose that atoms are located at the corners of the hexagon, and each atom has two electrons. The Wannier centers for four electrons, which are compatible with the lattice symmetry and the condition $w_2 = 1$, are then given by $(0, 0)$, $(0, a_2/2)$, $(a_1/2, a_2/2)$, and $(a_1/2, 0)$, respectively, where $(0, 0)$ indicates the center of the hexagon as shown in Fig. 9(c). Because of the nontrivial Wannier centers associated with the bulk invariant $w_2 = 1$, a mirror-invariant configuration of electrons must induce additional half charges at the mirror-invariant corners. When there is $M_y : y \rightarrow -y$ symmetry, the rightmost and leftmost unit cells on the M_y -invariant line have additional half charge induced by the bulk. Since any mirror-symmetric configuration of electrons adds integer charges to the mirror invariant line, additional half charges must be there. A similar argument holds for $M_x : x \rightarrow -x$ symmetric case. As in Su-Schrieffer-Heeger model [58–60], $C_{2z}T$ symmetry is broken by the corner charge, because we require the corner charge to be localized at one of the two corners. [See Appendix C for detailed model calculations for corner charges.]

In twisted bilayer graphene, $C_{6z}T$ and C_{2x} symmetries are generators of the approximate D_{6h} symmetry of the Moiré superlattice. $C_{2x} : (t, x, y) \rightarrow (t, x, -y)$ and $C_{2x}(C_{6z}T)^3 : (t, x, y) \rightarrow (-t, -x, y)$ operate like M_y and M_xT symmetries in two dimensions. Since M_xT plays the same role as M_x for protection of corner charges [62], anomalous corner charges may appear at either M_y -invariant corners or M_x -invariant corners. Although there is no chiral symmetry in TBG, the in-gap states may be robust due to the large band gap relative to the bandwidth of the nearly flat bands.

IX. DISCUSSION

We have shown that the Euler class e_2 of real two band systems with I_{ST} symmetry is identical to the total winding number $2e_2$ of the band degeneracies between two bands. Namely, the topological charge of band crossing points determines the global band topology. We expect that our theory here can be generalized to a broader class of systems. For instance, recently, a no-go theorem was proposed in [57]: the statement is that Wannier obstruction of a single band can only come from a nontrivial first Chern number. This implies that Wannier obstructions originating from the other topological invariants describing multi-band systems may require unremovable band degeneracies. It would be an interesting topic for future studies to establish the general relationship between the symmetry eigenvalues at high symmetry points, the topological charge of band degeneracies and the global band topology in crystalline topological materials.

Note added.— During the preparation of our manuscript, we have found related works [64, 65]. In [64], based on first-principles calculations, it was found that the Wilson loop

spectrum for nearly flat bands in twisted bilayer graphene has nontrivial winding, which is consistent with our conclusion. In [65], tight-binding models were constructed explicitly by adding trivial bands to the two nearly flat bands, which demonstrates the fragility of the Wannier obstruction for the flat bands.

ACKNOWLEDGMENTS

J.A. acknowledges the helpful discussions with Aris Alexandradianata and Yoonseok Hwang. J.A. and S.P. were supported by IBS-R009-D1. B.-J.Y. was supported by the Institute for Basic Science in Korea (Grant No. IBS-R009-D1) and Basic Science Research Program through the National Research Foundation of Korea (NRF) (Grant No. 0426-20170012, No.0426-20180011), and the POSCO Science Fellowship of POSCO TJ Park Foundation (No.0426-20180002). This work was supported in part by the U.S. Army Research Office under Grant Number W911NF-18-1-0137.

Appendix A: Winding number in general chiral symmetric systems

In the main text, we showed that the winding number can be computed using the off-diagonal Berry phase for I_{ST} -symmetric two bands. Notice that I_{ST} -symmetric two band Hamiltonian have chiral symmetry when the chemical potential term, which is irrelevant for the band crossing, is neglected. Here we show that the same method can be applied to any chiral symmetric systems.

1. Sewing matrix and Berry phase

Consider the sewing matrix for chiral symmetry operator S :

$$S_{mn}(\mathbf{k}) \equiv \langle u_{m\mathbf{k}} | S | u_{n\mathbf{k}} \rangle. \quad (\text{A1})$$

It takes an off-diagonal form

$$S(\mathbf{k}) = \begin{pmatrix} 0 & s^{-1}(\mathbf{k}) \\ s(\mathbf{k}) & 0 \end{pmatrix} \quad (\text{A2})$$

in the basis

$$|u_{\mathbf{k}}\rangle = \begin{pmatrix} |u_{\mathbf{k}}^{\text{unocc}}\rangle \\ |u_{\mathbf{k}}^{\text{occ}}\rangle \end{pmatrix}, \quad (\text{A3})$$

where $s(\mathbf{k}) \in U(N)$. The Berry connection

$$A_{mn}(\mathbf{k}) = \langle u_{m\mathbf{k}} | \nabla_{\mathbf{k}} | u_{n\mathbf{k}} \rangle \quad (\text{A4})$$

in chiral symmetric systems satisfies

$$\mathbf{A}(\mathbf{k}) = S^{-1}(\mathbf{k})\mathbf{A}(\mathbf{k})S(\mathbf{k}) + S^{-1}(\mathbf{k})\nabla_{\mathbf{k}}S(\mathbf{k}), \quad (\text{A5})$$

which shows that

$$\mathbf{A}_2(\mathbf{k}) = s\mathbf{A}_1(\mathbf{k})^{-1}s + s(\mathbf{k})\nabla_{\mathbf{k}}s^{-1}(\mathbf{k}), \quad (\text{A6})$$

and

$$\mathbf{a}(\mathbf{k}) \equiv i\mathbf{A}_{12}(\mathbf{k})s(\mathbf{k}) = (i\mathbf{A}_{12}(\mathbf{k})s(\mathbf{k}))^\dagger = \mathbf{a}^\dagger(\mathbf{k}). \quad (\text{A7})$$

Accordingly, the Berry connection takes the following form.

$$\mathbf{A}(\mathbf{k}) = \begin{pmatrix} \mathbf{A}_1(\mathbf{k}) & -i\mathbf{a}(\mathbf{k})s^{-1}(\mathbf{k}) \\ -is(\mathbf{k})\mathbf{a}(\mathbf{k}) & s\mathbf{A}_1(\mathbf{k})^{-1}s + s(\mathbf{k})\nabla_{\mathbf{k}}s^{-1}(\mathbf{k}) \end{pmatrix}, \quad (\text{A8})$$

where $\mathbf{A}_1(\mathbf{k})$ and $\mathbf{a}(\mathbf{k})$ are undetermined by the sewing matrix for chiral symmetry.

Under a gauge transformation $|u_{n\mathbf{k}}\rangle \rightarrow |u'_{n\mathbf{k}}\rangle = U_{mn}(\mathbf{k})|u_{m\mathbf{k}}\rangle$, the sewing matrix transforms as

$$S(\mathbf{k}) \rightarrow S'(\mathbf{k}) = U^\dagger(\mathbf{k})S(\mathbf{k})U(\mathbf{k}). \quad (\text{A9})$$

Accordingly, under a diagonal gauge transformation

$$U(\mathbf{k}) = \begin{pmatrix} U_1(\mathbf{k}) & 0 \\ 0 & U_2(\mathbf{k}) \end{pmatrix}, \quad (\text{A10})$$

$$s^{-1}(\mathbf{k}) \rightarrow s'^{-1}(\mathbf{k}) = U_1^\dagger(\mathbf{k})s^{-1}(\mathbf{k})U_2(\mathbf{k}). \quad (\text{A11})$$

Since the Berry connection transforms by

$$\mathbf{A}_{12}(\mathbf{k}) \rightarrow \mathbf{A}'_{12}(\mathbf{k}) = U_1^\dagger(\mathbf{k})\mathbf{A}_{12}(\mathbf{k})U_2(\mathbf{k}), \quad (\text{A12})$$

we get

$$\mathbf{a}(\mathbf{k}) \rightarrow \mathbf{a}'(\mathbf{k}) = U_1^\dagger(\mathbf{k})\mathbf{a}(\mathbf{k})U_1(\mathbf{k}). \quad (\text{A13})$$

Notice that the matrix trace of any power of $\mathbf{a}(\mathbf{k})$ is gauge invariant. It suggests that $\oint_{S^d} \text{Tr}[\mathbf{a}^d(\mathbf{k})]$ may serve as a d -dimensional topological invariant.

2. Winding number and the off-diagonal Berry phase

Suppose that the unoccupied and occupied bands are topologically trivial as a whole. Then there exists a Hamiltonian which is smooth over the whole Brillouin zone that describes both the unoccupied and occupied bands. When the chiral operator is represented by

$$S = \begin{pmatrix} 1_{N \times N} & 0 \\ 0 & -1_{N \times N} \end{pmatrix}, \quad (\text{A14})$$

the chiral-symmetric Hamiltonian takes the form of

$$\begin{aligned} H(\mathbf{k}) &= \begin{pmatrix} 0 & h(\mathbf{k}) \\ h^\dagger(\mathbf{k}) & 0 \end{pmatrix} \\ &= \begin{pmatrix} 0 & U(\mathbf{k})P(\mathbf{k}) \\ P(\mathbf{k})U^\dagger(\mathbf{k}) & 0 \end{pmatrix}, \end{aligned} \quad (\text{A15})$$

where we used polar decomposition of $h(\mathbf{k})$, where $U(\mathbf{k}) \in U(N)$ and $P(\mathbf{k}) = \sqrt{h^\dagger(\mathbf{k})h(\mathbf{k})}$. The energy eigenstates on gapped regions are given by

$$\begin{aligned} |u_{n\mathbf{k}}^{\text{unocc}}\rangle &= \frac{1}{\sqrt{2}} \begin{pmatrix} U(\mathbf{k})|e_{n\mathbf{k}}\rangle \\ |e_{n\mathbf{k}}\rangle \end{pmatrix}, \\ |u_{n\mathbf{k}}^{\text{occ}}\rangle &= \frac{1}{\sqrt{2}} \begin{pmatrix} U(\mathbf{k})|e_{n\mathbf{k}}\rangle \\ -|e_{n\mathbf{k}}\rangle \end{pmatrix}, \end{aligned} \quad (\text{A16})$$

where $|e_{n=1,\dots,N,\mathbf{k}}\rangle$ are the eigenstates of $P(\mathbf{k})$ with eigenvalues $|E_{n\mathbf{k}}|$, and $|u_{n\mathbf{k}}^{\text{unocc}}\rangle$ and $|u_{n\mathbf{k}}^{\text{occ}}\rangle$ have energies $|E_{n\mathbf{k}}|$ and $-|E_{n\mathbf{k}}|$, respectively.

In this choice of gauge, the Berry connection is given by

$$\begin{aligned} \mathbf{A}(\mathbf{k}) &= \begin{pmatrix} \frac{1}{2}U^\dagger(\mathbf{k})\nabla_{\mathbf{k}}U(\mathbf{k}) & (-i)\frac{i}{2}U^\dagger(\mathbf{k})\nabla_{\mathbf{k}}U(\mathbf{k}) \\ (-i)\frac{i}{2}U^\dagger(\mathbf{k})\nabla_{\mathbf{k}}U(\mathbf{k}) & \frac{1}{2}U^\dagger(\mathbf{k})\nabla_{\mathbf{k}}U(\mathbf{k}) \end{pmatrix} \\ &+ \begin{pmatrix} \langle e_{\mathbf{k}}|\nabla_{\mathbf{k}}|e_{\mathbf{k}}\rangle & 0 \\ 0 & \langle e_{\mathbf{k}}|\nabla_{\mathbf{k}}|e_{\mathbf{k}}\rangle \end{pmatrix}. \end{aligned} \quad (\text{A17})$$

From this expression, we see that

$$\mathbf{a}(\mathbf{k}) = \frac{i}{2}U^\dagger(\mathbf{k})\nabla_{\mathbf{k}}U(\mathbf{k}) = \frac{i}{2}\nabla_{\mathbf{k}}\log\det U(\mathbf{k}), \quad (\text{A18})$$

such that

$$\oint_{S^1} d\mathbf{k} \cdot \text{Tr}[\mathbf{a}(\mathbf{k})] = \frac{1}{2} \oint_{S^1} d\mathbf{k} \cdot \nabla_{\mathbf{k}}\theta(\mathbf{k}) = N_w\pi, \quad (\text{A19})$$

where $\det U(\mathbf{k}) = \exp(-i\theta(\mathbf{k}))$. This off-diagonal Berry phase is invariant under gauge transformations which do not mix the unoccupied and occupied bands. As in the main text, the sign of the winding number is fixed after we choose the global sign of $\text{Tr}[\mathbf{a}(\mathbf{k})]$.

In general, the winding number in $(2n+1)$ -dimensional chiral symmetric systems is given by

$$N_w^{(2n+1)} = \frac{(-1)^n n!}{(2n+1)!\pi^{n+1}} \oint_{S^{2n+1}} d^{2n+1}k \text{Tr}[(\mathbf{a}(\mathbf{k}))^{2n+1}]. \quad (\text{A20})$$

3. Space-time symmetries

Let us investigate the space-time symmetry constraint on $\mathbf{a}(\mathbf{k})$. It will turn out that $\mathbf{a}(\mathbf{k})$ transforms like a Berry curvature rather than a Berry connection. We get the same conclusion for I_{ST} -symmetric two bands because they have effective chiral symmetry if we neglect the chemical potential.

First we consider a crystalline symmetry operator G , where

$$G_{mn}(\mathbf{k}) \equiv \langle u_{mG\mathbf{k}}|G|u_{n\mathbf{k}}\rangle. \quad (\text{A21})$$

It takes the form

$$G(\mathbf{k}) = \begin{pmatrix} g_1(\mathbf{k}) & 0 \\ 0 & g_2(\mathbf{k}) \end{pmatrix} \quad (\text{A22})$$

in the basis

$$|u_{\mathbf{k}}\rangle = \begin{pmatrix} |u_{\mathbf{k}}^{\text{unocc}}\rangle \\ |u_{\mathbf{k}}^{\text{occ}}\rangle \end{pmatrix}, \quad (\text{A23})$$

where $g_{1,2}(\mathbf{k}) \in U(N)$. The symmetry constraint for the Berry connection is given by

$$\mathbf{A}(\mathbf{k}) = G^{-1}(\mathbf{k})P_G^{-1} \cdot \mathbf{A}(P_G\mathbf{k})G(\mathbf{k}) + G^{-1}(\mathbf{k})\nabla_{\mathbf{k}}G(\mathbf{k}), \quad (\text{A24})$$

where P_G^{-1} is the point group part of G , and $P_G^{-1} \cdot \mathbf{A}$ indicates the transformation of vector components of \mathbf{A} under the action of G . Then,

$$\mathbf{A}_i(\mathbf{k}) = g_i^{-1}(\mathbf{k})P_G^{-1} \cdot \mathbf{A}_i(P_G\mathbf{k})g_i(\mathbf{k}) + g_i^{-1}(\mathbf{k})\nabla_{\mathbf{k}}g_i(\mathbf{k}), \quad (\text{A25})$$

where $A_1 \equiv A_{11}$ and $A_2 \equiv A_{22}$, and

$$\mathbf{A}_{12}(\mathbf{k}) = g_1^{-1}(\mathbf{k})P_G^{-1} \cdot \mathbf{A}_{12}(P_G\mathbf{k})g_2(\mathbf{k}). \quad (\text{A26})$$

Because $[S, G] = 0$ requires that

$$G(\mathbf{k})S(\mathbf{k}) = S(G\mathbf{k})G(\mathbf{k}), \quad (\text{A27})$$

so that

$$s^{-1}(\mathbf{k}) = g_1^{-1}(\mathbf{k})s^{-1}(P_G\mathbf{k})g_2(\mathbf{k}), \quad (\text{A28})$$

we get

$$\begin{aligned} \mathbf{a}(\mathbf{k}) &= g_1^{-1}(\mathbf{k})P_G^{-1} \cdot \mathbf{a}(P_G\mathbf{k})g_1(\mathbf{k}) \\ &= g_2^{-1}(\mathbf{k})P_G^{-1} \cdot \mathbf{a}(P_G\mathbf{k})g_2(\mathbf{k}). \end{aligned} \quad (\text{A29})$$

Next we consider the time-reversal symmetry operator T , where

$$B_{mn}(\mathbf{k}) \equiv \langle u_{m-\mathbf{k}} | T | u_{n\mathbf{k}} \rangle. \quad (\text{A30})$$

It takes the form

$$B(\mathbf{k}) = \begin{pmatrix} b_1(\mathbf{k}) & 0 \\ 0 & b_2(\mathbf{k}) \end{pmatrix} \quad (\text{A31})$$

in the basis

$$|u_{\mathbf{k}}\rangle = \begin{pmatrix} |u_{\mathbf{k}}^{\text{unocc}}\rangle \\ |u_{\mathbf{k}}^{\text{occ}}\rangle \end{pmatrix}, \quad (\text{A32})$$

where $b_{1,2}(\mathbf{k}) \in U(N)$. The symmetry constraint for the Berry connection is given by

$$\mathbf{A}(-\mathbf{k}) = B(\mathbf{k})\mathbf{A}^*(\mathbf{k})B^{-1}(\mathbf{k}) + B(\mathbf{k})\nabla_{\mathbf{k}}B^{-1}(\mathbf{k}). \quad (\text{A33})$$

Then,

$$\mathbf{A}_i(-\mathbf{k}) = b_i(\mathbf{k})\mathbf{A}_i(\mathbf{k})b_i^{-1}(\mathbf{k}) + b_i(\mathbf{k})\nabla_{\mathbf{k}}b_i^{-1}(\mathbf{k}), \quad (\text{A34})$$

where $A_1 \equiv A_{11}$ and $A_2 \equiv A_{22}$, and

$$\mathbf{A}_{12}(-\mathbf{k}) = b_1(\mathbf{k})\mathbf{A}_{12}^*(\mathbf{k})b_2^{-1}(\mathbf{k}). \quad (\text{A35})$$

Because $[S, T] = 0$ requires that

$$B(\mathbf{k})S^*(\mathbf{k}) = S(-\mathbf{k})B(\mathbf{k}), \quad (\text{A36})$$

so that

$$s^{-1}(-\mathbf{k}) = b_1(\mathbf{k})(s^{-1})^*(\mathbf{k})b_2^{-1}(\mathbf{k}), \quad (\text{A37})$$

we get

$$\begin{aligned} \mathbf{a}(-\mathbf{k}) &= b_1(\mathbf{k})\mathbf{a}^*(\mathbf{k})b_1^{-1}(\mathbf{k}) \\ &= b_2(\mathbf{k})\mathbf{a}^*(\mathbf{k})b_2^{-1}(\mathbf{k}). \end{aligned} \quad (\text{A38})$$

Appendix B: Equivalence of the second Stiefel-Whitney class and the Fu-Kane-Mele invariant

In spin-orbit coupled 2D systems with time reversal T and two-fold rotation C_{2z} symmetries, both the second Stiefel-Whitney class and the Fu-Kane-Mele invariant are protected, respectively by $C_{2z}T$ and T . As we mentioned in the main text, the Wilson loop method implies that the second Stiefel-Whitney class is identical to the Z_2 topological variant, because they are characterized by the same pattern of the Wilson loop spectral flow. Here we provide another proof of the equivalence using the Euler class and the Fu-Kane-Mele invariant. Our proof here goes parallel with the derivation of the relation between the second Stiefel-Whitney class and inversion eigenvalues, presented in Supplemental Material of [42].

We first notice that the total Berry phase of the occupied bands is always nontrivial in this system because the Berry phase is quantized to be a multiple of π due to the $C_{2z}T$ symmetry, but T further requires it be a multiple of 2π because energy bands form Kramers pairs [40]. Therefore, the occupied states are always orientable in a real gauge, so we take transition functions belonging to the special orthogonal group. Furthermore, we will only consider two occupied bands because we can block-diagonalize the sewing matrix B into 2×2 blocks by lifting the accidental degeneracy of occupied bands without loss of generality.

Let us take a real gauge: $C_{2z}T|\tilde{u}_{n\mathbf{k}}\rangle = |\tilde{u}_{n\mathbf{k}}\rangle$. Time reversal symmetry imposes a further constraint on energy eigenstates by

$$T|u_{n\mathbf{k}}^B\rangle = B_{mn}^{AB}(\mathbf{k})|u_{m-\mathbf{k}}^A\rangle, \quad (\text{B1})$$

where $B(\mathbf{k}) \in O(2)$ is the sewing matrix for time reversal, and A and B denotes the local patch on which the states are smoothly defined.

In fact, the sewing matrix B belongs to $SO(2)$. In general, as the real occupied states are not smooth over the whole 2D Brillouin zone, the sewing matrix also is not smooth. The sewing matrix defined on C and D patches are related to the one defined on A and B patches as

$$B^{CD}(\mathbf{k}) = (t^{AC}(-\mathbf{k}))^{-1}B^{AB}(\mathbf{k})t^{BD}(\mathbf{k}), \quad (\text{B2})$$

where A and C covers $-\mathbf{k}$, and B and D covers \mathbf{k} , and t^{AB} and t^{CD} are the transition functions defined by $|u_{n-\mathbf{k}}^C\rangle = t_{mn}^{AC}(-\mathbf{k})|u_{n-\mathbf{k}}^A\rangle$ and $|u_{n\mathbf{k}}^D\rangle = t_{mn}^{BD}(\mathbf{k})|u_{n\mathbf{k}}^B\rangle$. Since we required all the transition functions be orientation-preserving, the above relation shows that the determinant of the sewing matrix is uniform: $\det B_{CD} = \det(t^{AC})^{-1} \det B_{AB} \det t^{BD} = \det B_{AB}$. Because $B = \pm i\sigma_y$ at time-reversal-invariant momenta (TRIM), such that $\det B = 1$ at TRIM, the sewing matrix belongs to $SO(2)$ everywhere on the Brillouin zone.

The symmetry constraint on the Berry connection and curvature

$$\begin{aligned} \tilde{\mathbf{A}}(\mathbf{k}) &= -B^T(\mathbf{k})\tilde{\mathbf{A}}(-\mathbf{k})B(\mathbf{k}) - B^T(\mathbf{k})\nabla_{\mathbf{k}}B(\mathbf{k}), \\ \tilde{\mathbf{F}}(\mathbf{k}) &= B^T(\mathbf{k})\tilde{\mathbf{F}}(-\mathbf{k})B(\mathbf{k}). \end{aligned} \quad (\text{B3})$$

reduce to

$$\begin{aligned}\tilde{\mathbf{A}}(\mathbf{k}) + \tilde{\mathbf{A}}(-\mathbf{k}) &= \begin{pmatrix} 0 & -\nabla_{\mathbf{k}}\phi(\mathbf{k}) \\ \nabla_{\mathbf{k}}\phi(\mathbf{k}) & 0 \end{pmatrix}, \\ \tilde{\mathbf{F}}(\mathbf{k}) &= \tilde{\mathbf{F}}(-\mathbf{k}),\end{aligned}\quad (\text{B4})$$

where

$$B(\mathbf{k}) = \begin{pmatrix} \cos \phi(\mathbf{k}) & \sin \phi(\mathbf{k}) \\ -\sin \phi(\mathbf{k}) & \cos \phi(\mathbf{k}) \end{pmatrix}. \quad (\text{B5})$$

Because the Fu-Kane-Mele invariant Δ is defined by the change of a 1D quantity, the time reversal polarization P_T , let us first investigate the 1D topological invariant. Consider a time-reversal-invariant 1D subBrillouin zone, which includes two TRIM Γ_1 and Γ_2 . We can take a real smooth gauge there because the first Stiefel-Whitney class is trivial, i.e., the total Berry phase is trivial in complex smooth gauges as explained above. On the time-reversal-invariant 1D Brillouin zone, we observe from symmetry conditions that

$$\begin{aligned}\oint d\mathbf{k} \cdot \tilde{\mathbf{A}}_{12}(\mathbf{k}) &= \int_{\Gamma_1}^{\Gamma_2} d\mathbf{k} \cdot (\tilde{\mathbf{A}}_{12}(\mathbf{k}) + \tilde{\mathbf{A}}_{12}(-\mathbf{k})) \\ &= - \int_{\Gamma_1}^{\Gamma_2} d\mathbf{k} \cdot \nabla_{\mathbf{k}}\phi(\mathbf{k}) \\ &= i \log \frac{\text{Pf}B(\Gamma_2)}{\text{Pf}B(\Gamma_1)} \text{ mod } 2\pi \\ &= 2\pi P_T \text{ mod } 2\pi,\end{aligned}\quad (\text{B6})$$

where we used the definition of the time-reversal polarization in the last step [66]. This integral is defined only modulo 2π because a gauge transformation can change its value by 2π times an integer [67].

Now we return to the original 2D Brillouin zone. Let us take a real gauge where the occupied states are smooth over the region including the half Brillouin zone $0 \leq k_x \leq \pi$. The Fu-Kane-Mele invariant Δ is defined as the time-reversal polarization pump from $k_x = 0$ to $k_x = \pi$, i.e., $\Delta = P_T(\pi) - P_T(0)$, so

$$\begin{aligned}\Delta &= \frac{1}{2\pi} \left(i \log \frac{\text{Pf}B(\pi, \pi)}{\text{Pf}B(\pi, 0)} - i \log \frac{\text{Pf}B(0, \pi)}{\text{Pf}B(0, 0)} \right) \\ &= \frac{1}{2\pi} \oint dk_y \tilde{A}_{12,y}(\pi, k_y) - \frac{1}{2\pi} \oint dk_y \tilde{A}_{12,y}(0, k_y) \\ &= \frac{1}{2\pi} \int_0^\pi dk_x \int_{-\pi}^\pi dk_y \tilde{F}_{12,z}(k_x, k_y) \\ &= \frac{1}{4\pi} \int_{-\pi}^\pi dk_x \int_{-\pi}^\pi dk_y \tilde{F}_{12,z}(k_x, k_y) \\ &= \frac{1}{2} e_2 = \frac{1}{2} w_2 \text{ mod } 1,\end{aligned}\quad (\text{B7})$$

where we used $\tilde{\mathbf{F}}(-\mathbf{k}) = \tilde{\mathbf{F}}(\mathbf{k})$ in the fourth line. This shows the equivalence of the (two times) Fu-Kane-Mele invariant Δ and the second Stiefel-Whitney class w_2 .

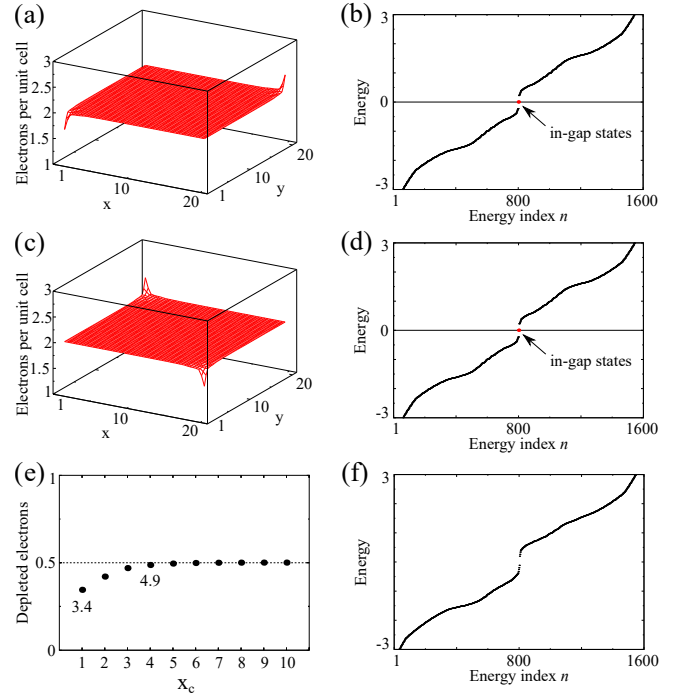


FIG. 10. Corner charges in model Eq. (C1). Finite-size calculations are done by transforming the momentum space Hamiltonian into a square lattice tight-binding model, which has 20 by 20 unit cells. To get a definite sign of the corner charges, inversion symmetry is slightly broken by including a local chemical potential shift μ at corners. (a,b) M_{x+y} symmetric case. $m_1 = m_3 = 0.4$ and $m_2 = m_4 = 0.2$. $\mu = 0.01$ at $(x, y) = (1, 1)$. (c,d) M_{x-y} symmetric case. $m_1 = -m_3 = 0.4$ and $m_2 = -m_4 = 0.2$. $\mu = 0.01$ at $(x, y) = (20, 0)$. (e) Depleted electrons near the corner $(x, y) = (1, 1)$ in (a). It is calculated from $\sum_{x=1}^{x_c} \sum_{y=1}^{y_c} \langle \rho(x, y) \rangle - \rho(x, y)$, where $\rho(x, y)$ is the number of electrons in the unit cell at (x, y) , and $\langle \rho(x, y) \rangle = 2$. (f) In the absence of mirror symmetry. $m_1 = 0.1$, $m_3 = 0.4$ and $m_2 = m_4 = 0.2$. No in-gap states appear in this case.

Appendix C: Protection and characterization the second-order topology

Recently, Wang *et al.* proposed in [56] that the anomalous corner charges are induced by the nontrivial second Stiefel-Whitney class. Here we will deal with issues that was not fully covered in [56]. First, we specify which symmetries protect the anomalous corner charges. We demonstrate that mirror and chiral symmetries are essential for the protection of corner charges, using the same model introduced in [56]. Then, we discuss on the meaning of the nested Wilson loop method that was introduced in [56] to capture the existence of the anomalous corner charges.

1. Mirror and chiral symmetries

The model introduced in [56] has the following form.

$$H = \sin k_x \Gamma_1 + \sin k_y \Gamma_2 + (-3 + \cos k_x + \cos k_y) \Gamma_3 + m_1 \Gamma_{14} + m_2 \Gamma_{15} + m_3 \Gamma_{24} + m_4 \Gamma_{25}, \quad (C1)$$

where we defined three real Gamma matrices

$$\Gamma_1 = \tau_x, \quad \Gamma_2 = \tau_y \sigma_y, \quad \Gamma_3 = \tau_z, \quad (C2)$$

and two pure imaginary Gamma matrices

$$\Gamma_4 = \tau_y \sigma_x, \quad \Gamma_5 = \tau_y \sigma_z, \quad (C3)$$

and the other generators of real matrices are then

$$\begin{aligned} \Gamma_{14} &= \tau_z \sigma_x, & \Gamma_{15} &= \tau_z \sigma_z, \\ \Gamma_{24} &= -\sigma_z, & \Gamma_{25} &= \sigma_x, \\ \Gamma_{34} &= -\tau_x \sigma_x, & \Gamma_{35} &= -\tau_y \sigma_z. \end{aligned} \quad (C4)$$

The Hamiltonian is symmetric under

$$P = \Gamma_3, \quad T = \Gamma_3 K. \quad (C5)$$

$PT = K$ symmetry requires the Hamiltonian be real.

In [56], anomalous in-gap states were demonstrated with parameters, $m_1 = 0.3$, $m_3 = 0.4$, and $m_2 = m_4 = 0.2$. Let us note that this set of parameters are very close to the mirror and chiral symmetric parameters. When $m_1 = m_3$ and $m_2 = m_4$, the Hamiltonian Eq. (C1) has chiral S and two mirror $M_{x+y} : (x, y) \rightarrow (-y, -x)$ and $M_{x-y} : (x, y) \rightarrow (y, x)$ symmetries in addition to spatial inversion and time reversal symmetries. To see this, let us rewrite the above Hamiltonian as

$$\begin{aligned} H &= \frac{1}{2}(\sin k_x + \sin k_y)(\Gamma_1 + \Gamma_2) \\ &+ \frac{1}{2}(\sin k_x - \sin k_y)(\Gamma_1 - \Gamma_2) \\ &+ (-3 + \cos k_x + \cos k_y) \Gamma_3 \\ &- i(\Gamma_1 + \Gamma_2)(m_1 \Gamma_4 + m_2 \Gamma_5). \end{aligned} \quad (C6)$$

In this form, one can see that it is symmetric under

$$\begin{aligned} M_{x+y} &= \frac{i}{\sqrt{2m^2}}(\Gamma_1 + \Gamma_2)(m_1 \Gamma_4 + m_2 \Gamma_5), \\ M_{x-y} &= \frac{i}{\sqrt{2m^2}}(\Gamma_1 - \Gamma_2)(m_1 \Gamma_4 - m_2 \Gamma_5)(m_1 \Gamma_4 + m_2 \Gamma_5), \\ S &= \frac{1}{\sqrt{m^2}}(m_1 \Gamma_4 + m_2 \Gamma_5) \end{aligned} \quad (C7)$$

where $m^2 = m_1^2 + m_2^2$. $M_{x+y}^2 = M_{x-y}^2 = S^2 = 1$, and M_{x+y} , M_{x-y} , and S all commutes with time reversal T .

While M_{x+y} anticommutes with S , M_{x-y} commutes with S . Therefore, M_{x+y} and M_{x-y} belongs to the $\text{BDI}^{\mathcal{M}+-}$ and $\text{BDI}^{\mathcal{M}++}$ classes, which are classified by \mathbb{Z} and 0, respectively [62]. The subscript in \mathcal{M}_{+-} represents commutation (+) and anti-commutation (-) relation of the mirror operation

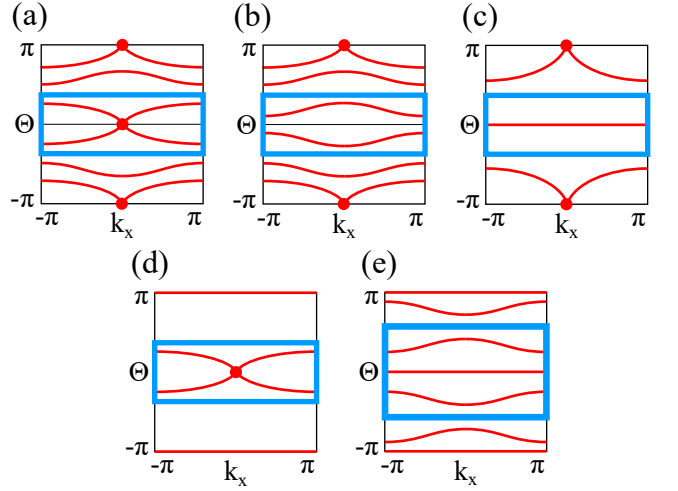


FIG. 11. Wilson loop spectrum with the nontrivial second Stiefel-Whitney class ($w_2 = 1$). $\Theta(k_x)$ is the phase eigenvalue of the Wilson loop operator calculated along k_y at fixed k_x . Blue boxes show the block of Wilson bands chosen for the calculation of the nested Wilson loop W_2 along k_x . (a) $(\Phi_x, \Phi_y) = (0, 0)$. $\det W_2 = -1$. (b) $(\Phi_x, \Phi_y) = (\pi, 0)$. $\det W_2 = +1$. (c) $(\Phi_x, \Phi_y) = (0, 0)$ or $(\pi, 0)$. $\det W_2 = \pm 1$. (d) $(\Phi_x, \Phi_y) = (0, \pi)$ or (π, π) . $\det W_2 = -1$. (e) $(\Phi_x, \Phi_y) = (0, \pi)$ or (π, π) . $\det W_2 = -1$. Here Φ_x and Φ_y are the Berry phases for the whole bands (usually the occupied bands) along k_x and k_y . The nested Wilson loop method in [56] applies to (a,b,e) but not to (c,d).

with time reversal T and particle-hole TS operations, respectively.

According to the K-theory classification, corner charges are accumulated at the M_{x-y} -invariant corners when $m_1 = m_3$ and $m_2 = m_4$. This is consistent with our calculations in Fig. 10(a,b). Also, if we choose parameters $m_1 = -m_3$ and $m_2 = -m_4$, corner charges are accumulated at M_{x+y} -invariant corners as shown in Fig. 10(c,d) since then the role of M_{x+y} and M_{x-y} is changed. The corner states carry half charges as shown in Fig. 10(e). Those in-gap states disappear when mirror and chiral symmetries are broken [See Fig. 10(f)].

2. Nested Wilson loop method

The nested Wilson loop method was proposed in [56] as a diagnostic for anomalous corner charges induced from the bulk topology. This method was introduced as follows. First, one calculates the Wilson loop operator along k_y as a function of k_x (Here, k_x and k_y are arbitrary two independent momenta that parametrizes the 2D Brillouin zone.). Then, its phase eigenvalues Θ 's (so-called Wilson bands) are calculated. The spectrum is gapped in general except for possible crossings at $\Theta = 0$ or $\Theta = \pi$, because only crossings at $\Theta = 0$ and $\Theta = \pi$ are protected by I_{ST} symmetry [42] [See Fig. 11]. Therefore, one can separate the Wilson bands into two groups that are centered at $\Theta = 0$ and $\Theta = \pi$, respectively. This choice is not unique, and the number of bands in a group can

vary depending on the choice. Then, we select the group of bands near $\Theta = 0$, and calculate their determinant of the Wilson loop along k_x , i.e., the exponentiation of the Berry phase for the group of bands along k_x . It was suggested that this determinant of the “nested Wilson loop” is -1 ($+1$) when an anomalous corner charge is (not) present. This method applies only to the cases when the number of bands is bigger than two because the Wilson loop spectrum is not gapped in general for two bands. See Fig. 1(d) in the main text as an example of a gapless Wilson loop spectrum for two bands.

Let us clarify here how the nested Wilson loop is related to the second Stiefel-Whitney class, which is responsible for the appearance of the anomalous corner charges. First, notice that decomposing the Wilson bands into two blocks \mathcal{B}_1 and \mathcal{B}_2 (which are centered at $\Theta = 0$ and $\Theta = \pi$, respectively) corresponds to decomposing the transition functions into two blocks, because the Wilson loop operator corresponds to transition functions in a parallel-transport gauge [42]. Therefore, according to the Whitney sum formula [42, 43], the total Stiefel-Whitney class can be given by the topological invariants of two blocks by

$$w_2(\mathcal{B}_1 \oplus \mathcal{B}_2) = w_2(\mathcal{B}_1) + w_2(\mathcal{B}_2) + \frac{1}{\pi^2} (\Phi_x(\mathcal{B}_1)\Phi_y(\mathcal{B}_2) + \Phi_x(\mathcal{B}_2)\Phi_y(\mathcal{B}_1)). \quad (\text{C8})$$

In this respect, the determinant of the nested Wilson loop $\det W_2$ calculates $\exp(i\Phi_x(\mathcal{B}_1))$. Moreover, $\Phi_y(\mathcal{B}_1) = 0$ since \mathcal{B}_1 is centered at $\Theta = 0$, and $w_2(\mathcal{B}_1) = 0$ since it is given by the number of the Wilson band crossing at $\Theta = \pi$ [42]. Thus we have

$$w_2(\mathcal{B}_1 \oplus \mathcal{B}_2) = w_2(\mathcal{B}_2) - \frac{i}{\pi^2} \log(\det W_2)\Phi_y(\mathcal{B}_2). \quad (\text{C9})$$

Moreover, $w_2(\mathcal{B}_2)$ and $\det W_2$ are further related to each other in some cases. In order to investigate all the possible cases with $w_2(\mathcal{B}_1 \oplus \mathcal{B}_2) = 1$, shown in Fig. 11, let us recall that the second Stiefel-Whitney class is calculated by the Wilson loop spectrum as follows [42]: when $\Phi_y = 0$, it is given by the number of crossing points at $\Theta = \pi$ [Fig. 11(a,b,c)],

and when $\Phi_y = \pi$, it is given by the number of crossing points at $\Theta = 0$ if the number of bands is odd [Fig. 11(d)] and it is undetermined by the spectrum if the number of bands is even [Fig. 11(e)]. Furthermore, the Berry phase along k_x direction can be determined by the parity of the number of crossing points between the Wilson loop spectrum, e.g., $\Phi_x = 0$ in Fig. 11(a) ($\Phi_x = \pi$ in Fig. 11(b)) because there are even (odd) crossing points in total. However, the Berry phase is indeterminate when there are flat Wilson bands at $\Theta = 0$ or π as in Fig. 11 (c),(d),(e). The same method can be applied to a subset of Wilson bands. With this in mind, let us consider the following two cases:

(1) When $\Phi_y(\mathcal{B}_2) = 0$ as shown in Fig. 11(a,b,c), we also have $w_2(\mathcal{B}_2) = 1$, so we automatically have $w_2(\mathcal{B}_1 \oplus \mathcal{B}_2) = 1$, regardless of $\det W_2$. Here $\det W_2 = -1$ and $+1$ in (a) and (b), respectively, but $\det W_2$ is indeterminate in (c). $\det W_2$ can be read from the number of the crossing at $\Theta = 0$: $\det W_2 = 1$ (-1) when the number is even (odd) [42]. When there is a flat Wilson band at $\Theta = 0$, $\det W_2$ is not determined by the spectrum, and one needs to calculate it directly. Thus, $w_2(\mathcal{B}_1 \oplus \mathcal{B}_2) = 1$ matches $\det W_2 = -1$ in (a) but not in (b) and (c).

(2) When $\Phi_y(\mathcal{B}_2) = \pi$ as shown in Fig. 11(d,e), $w_2(\mathcal{B}_2) = 0$ as the Wilson bands in \mathcal{B}_2 does not cross, so $w_2(\mathcal{B}_1 \oplus \mathcal{B}_2) = -\frac{i}{\pi} \log(\det W_2)$. $\det W_2 = -1$ gives $w_2(\mathcal{B}_1 \oplus \mathcal{B}_2) = 1$ in these cases. In (d), $\det W_2 = -1$ manifests as the odd number of crossing of Wilson bands at $\Theta = 0$. On the other hand, in (e), $\det W_2 = -1$ cannot be seen in the spectrum, so it should be directly calculated.

In conclusion, the determinant of the nested Wilson loop is equivalent to second Stiefel-Whitney class in the cases shown in Fig. 11(a,d,e). Especially in (e), the (non-nested) Wilson loop spectrum does not give any information on w_2 , so the nested Wilson loop should be calculated to get w_2 . In practice, however, one would not need the nested Wilson loop method. It is because we can determine w_2 directly from the Wilson loop spectrum without additionally calculating the nested Wilson loop in Fig. 11(a,d), and we can avoid (e) by calculating the Wilson loop along a different direction (along k_x or along $k_x + k_y$) to get (a) or (b).

-
- [1] Y. Cao, V. Fatemi, S. Fang, K. Watanabe, T. Taniguchi, E. Kaxiras, and P. Jarillo-Herrero, *Unconventional superconductivity in magic-angle graphene superlattices*, Nature **556**, 43 (2018).
- [2] Y. Cao, V. Fatemi, A. Demir, S. Fang, S. L. Tomarken, J. D. Luo, J. Y. and Sanchez-Yamagishi, K. Watanabe, T. Taniguchi, E. Kaxiras, *et al.*, *Correlated insulator behaviour at half-filling in magic-angle graphene superlattices*, Nature **556**, 80 (2018).
- [3] G. E. Volovik, *Graphite, graphene, and the flat band superconductivity*, JETP Letters **107**, 516–517 (2018).
- [4] C. Xu and L. Balents, *Topological superconductivity in twisted multilayer graphene*, arXiv:1803.08057 (2018).
- [5] B. Roy and V. Juricic, *Unconventional superconductivity in nearly flat bands in twisted bilayer graphene*, arXiv:1803.11190 (2018).
- [6] H. Guo, X. Zhu, S. Feng, and R. T. Scalettar, *Pairing symmetry of interacting fermions on twisted bilayer graphene superlattice*, arXiv:1804.00159 (2018).
- [7] G. Baskaran, *Theory of emergent josephson lattice in neutral twisted bilayer graphene (moiré is different)*, arXiv:1804.00627 (2018).
- [8] B. Padhi, C. Setty, and P. W. Phillips, *Wigner crystallization in lieu of mottness in twisted bilayer graphene*, arXiv:1804.01101 (2018).
- [9] V. Y. Irkhin and Y. N. Skryabin, *Dirac points, spinons and spin liquid in twisted bilayer graphene*, JETP Letters, 1–4 (2018).
- [10] J. F. Dodaro, S. A. Kivelson, Y. Schattner, X.-Q. Sun, and C. Wang, *Phases of a phenomenological model of twisted bilayer graphene*, arXiv:1804.03162 (2018).
- [11] T. Huang, L. Zhang, and T. Ma, *Antiferromagnetically ordered mott insulator and $d + id$ superconductivity in twisted bilayer graphene: A quantum monte carlo study*, arXiv:1804.06096 (2018).

- [12] L. Zhang, *Low-energy moiré band formed by dirac zero modes in twisted bilayer graphene*, arXiv:1804.09047 (2018).
- [13] S. Ray and T. Das, *Wannier pairs in the superconducting twisted bilayer graphene and related systems*, arXiv:1804.09674 (2018).
- [14] C.-C. Liu, L.-D. Zhang, W.-Q. Chen, and F. Yang, *Chiral sdw and $d+id$ superconductivity in the magic-angle twisted bilayer-graphene*, arXiv:1804.10009 (2018).
- [15] X. Y. Xu, K. T. Law, and Patrick A. Lee, *Kekulé valence bond order in an extended hubbard model on the honeycomb lattice, with possible applications to twisted bilayer graphene*, arXiv:1805.00478 (2018).
- [16] L. Rademaker and P. Mellado, *Charge-transfer insulation in twisted bilayer graphene*, arXiv:1805.05294 (2018).
- [17] H. Isobe, N. F. Q. Yuan, and L. Fu, *Superconductivity and charge density wave in twisted bilayer graphene*, arXiv:1805.06449 (2018).
- [18] F. Wu, A. H. MacDonald, and I. Martin, *Theory of phonon-mediated superconductivity in twisted bilayer graphene*, arXiv:1805.08735 (2018).
- [19] J. M. Pizarro, M. J. Calderón, and E. Bascones, *The nature of correlations in the insulating states of twisted bilayer graphene*, arXiv:1805.07303 (2018).
- [20] T. J. Peltonen, R. Ojajarvi, and T. T. Heikkilä, *Mean-field theory for superconductivity in twisted bilayer graphene*, arXiv:1805.01039 (2018).
- [21] Y.-Z. You and A. Vishwanath, *Superconductivity from valley fluctuations and approximate $SO(4)$ symmetry in a weak coupling theory of twisted bilayer graphene*, arXiv:1805.06867 (2018).
- [22] X.-C. Wu, K. A. Pawlak, C.-M. Jian, and C. Xu, *Emergent superconductivity in the weak mott insulator phase of bilayer graphene moiré superlattice*, arXiv:1805.06906 (2018).
- [23] H. K. Pal, *On magic angles and band flattening in twisted bilayer graphene*, arXiv:1805.08803 (2018).
- [24] M. Ochi, M. Koshino, and K. Kuroki, *Possible correlated insulating states in magic-angle twisted bilayer graphene under strongly competing interactions*, arXiv:1805.09606 (2018).
- [25] M. Fidrysiak, M. Zegrodnik, and J. Spałek, *Unconventional topological superconductivity and phase diagram for a two-orbital model of twisted bilayer graphene*, arXiv:1805.01179 (2018).
- [26] A. Thomson, S. Chatterjee, S. Sachdev, and M. S. Scheurer, *Triangular antiferromagnetism on the honeycomb lattice of twisted bilayer graphene*, Phys. Rev. B **98**, 075109 (2018).
- [27] F. Guinea and N. R. Walet, *Electrostatic effects and band distortions in twisted graphene bilayers*, arXiv:1806.05990 (2018).
- [28] L. Zou, H. C. Po, A. Vishwanath, and T. Senthil, *Band structure of twisted bilayer graphene: Emergent symmetries, commensurate approximants and wannier obstructions*, arXiv:1806.07873 (2018).
- [29] H. C. Po, L. Zou, A. Vishwanath, and T. Senthil, *Origin of mott insulating behavior and superconductivity in twisted bilayer graphene*, arXiv:1803.09742 (2018).
- [30] M. Koshino, N. F. Q. Yuan, M. Ochi, K. Kuroki, and L. Fu, *Maximally-localized wannier orbitals and the extended hubbard model for the twisted bilayer graphene*, arXiv:1805.06819 (2018).
- [31] N. F. Q. Yuan and L. Fu, *A model for metal-insulator transition in graphene superlattices and beyond*, arXiv:1803.09699 (2018).
- [32] J. Kang and O. Vafek, *Symmetry, maximally localized wannier states, and low energy model for the twisted bilayer graphene narrow bands*, arXiv:1805.04918 (2018).
- [33] J.M.B Lopes Dos Santos, N.M.R. Peres, and A.H. C. Neto, *Graphene bilayer with a twist: Electronic structure*, Phys. Rev. Lett. **99**, 256802 (2007).
- [34] R. Bistritzer and A. H. MacDonald, *Moiré bands in twisted double-layer graphene*, PNAS **108**, 12233–12237 (2011).
- [35] S. Shallcross, S. Sharma, E. Kandelaki, and O.A. Pankratov, *Electronic structure of turbostratic graphene*, Phys. Rev. B **81**, 165105 (2010).
- [36] E. S. Morell, J. Correa, P. Vargas, M. Pacheco, and Z. Barticevic, *Flat bands in slightly twisted bilayer graphene: Tight-binding calculations*, Phys. Rev. B **82**, 121407 (2010).
- [37] G. Trambly de Laissardiere, D. Mayou, and L. Magaud, *Localization of dirac electrons in rotated graphene bilayers*, Nano Lett. **10**, 804–808 (2010).
- [38] J. Jung, A. Raoux, Z. Qiao, and A. H. MacDonald, *Ab-initio theory of moiré superlattice bands in layered two-dimensional materials*, Phys. Rev. B **89**, 205414 (2014).
- [39] Y. Cao, J. Y. Luo, V. Fatemi, S. Fang, J.D. Sanchez-Yamagishi, K. Watanabe, T. Taniguchi, E. Kaxiras, and P. Jarillo-Herrero, *Superlattice-induced insulating states and valley-protected orbits in twisted bilayer graphene*, Phys. Rev. Lett. **117**, 116804 (2016).
- [40] J. Ahn and B.-J. Yang, *Unconventional topological phase transition in two-dimensional systems with space-time inversion symmetry*, Phys. Rev. Lett. **118**, 156401 (2017).
- [41] H. B. Nielsen and M. Ninomiya, *No-go theorem for regularizing chiral fermions*, Tech. Rep. (Science Research Council, 1981).
- [42] J. Ahn, Y. Kim, and B.-J. Yang, *Linking structure and band topology of nodal line semimetals with z_2 monopole charges*, arXiv:1803.11416 (2018).
- [43] A. Hatcher, *Vector bundles and K-theory*, <http://pi.math.cornell.edu/hatcher/VBKT/VB.pdf> (unpublished).
- [44] Y.X. Zhao and Y. Lu, *PT -symmetric real dirac fermions and semimetals*, Phys. Rev. Lett. **118**, 056401 (2017).
- [45] M. Nakahara, *Geometry, Topology and Physics* (CRC Press, 2003).
- [46] C. Fang, Y. Chen, H.-Y. Kee, and L. Fu, *Topological nodal line semimetals with and without spin-orbital coupling*, Phys. Rev. B **92**, 081201 (2015).
- [47] C. Brouder, G. Panati, M. Calandra, C. Mourougane, and N. Marzari, *Exponential localization of wannier functions in insulators*, Phys. Rev. Lett. **98**, 046402 (2007).
- [48] E. Witten, *Three lectures on topological phases of matter*, La Rivista del Nuovo Cimento **39**, 313 (2016).
- [49] C.-K. Chiu, J. C. Y. Teo, A. P. Schnyder, and S. Ryu, *Classification of topological quantum matter with symmetries*, Rev. Mod. Phys. **88**, 035005 (2016).
- [50] Notice that this is a generalization of the Poincaré-Hopf theorem [68], which relates zeros of vector fields to the Euler characteristic of the manifold, to non-tangent vector bundles.
- [51] P. Adrien M. Dirac, *Quantised singularities in the electromagnetic field*, Proc. R. Soc. Lond. A **133**, 60–72 (1931).
- [52] K. Sun, H. Yao, E. Fradkin, and S. A. Kivelson, *Topological insulators and nematic phases from spontaneous symmetry breaking in 2d fermi systems with a quadratic band crossing*, Phys. Rev. Lett. **103**, 046811 (2009).
- [53] G. Montambaux, L.-K. Lim, J.-No.ël Fuchs, and F. Piéchon, *Winding vector: how to annihilate two dirac points with the same charge*, arXiv:1804.00781 (2018).
- [54] J. Kruthoff, J. de Boer, and J. van Wezel, *Topology in time-reversal symmetric crystals*, arXiv:1711.04769 (2017).
- [55] H. C. Po, H. Watanabe, and A. Vishwanath, *Fragile topology*

- and wannier obstructions, arXiv:1709.06551 (2017).
- [56] Z. Wang, B. J. Wieder, J. Li, B. Yan, and B. A. Bernevig, *Higher-order topology, monopole nodal lines, and the origin of large fermi arcs in transition metal dichalcogenides xte_2 ($x=mo, w$)*, arXiv:1806.11116 (2018).
- [57] A. Alexandradinata and J. Höller, *No-go theorem for topological insulators and sure-fire recipe for chern insulators*, arXiv:1804.04131 (2018).
- [58] W. P. Su, J. R. Schrieffer, and A. J. Heeger, *Solitons in polyacetylene*, Phys. Rev. Lett. **42**, 1698 (1979).
- [59] W. A. Benalcazar, B. A. Bernevig, and T. L. Hughes, *Quantized electric multipole insulators*, Science **357**, 61–66 (2017).
- [60] W. A. Benalcazar, B. A. Bernevig, and T. L. Hughes, *Electric multipole moments, topological multipole moment pumping, and chiral hinge states in crystalline insulators*, Phys. Rev. B **96**, 245115 (2017).
- [61] S. Franca, J. Brink, and I. C. Fulga, *Anomalous higher-order topological insulators*, arXiv:1807.09050 (2018).
- [62] M. Geier, L. Trifunovic, M. Hoskam, and P. W. Brouwer, *Second-order topological insulators and superconductors with an order-two crystalline symmetry*, Phys. Rev. B **97**, 205135 (2018).
- [63] E. Khalaf, *Higher-order topological insulators and superconductors protected by inversion symmetry*, Phys. Rev. B **97**, 205136 (2018).
- [64] Z. Song, Z. Wang, W. Shi, G. Li, C. Fang, and B. A. Bernevig, *All “magic angles” are “stable” topological*, arXiv:1807.10676 (2018).
- [65] H. C. Po, L. Zou, T. Senthil, and A. Vishwanath, *Faithful tight-binding models and fragile topology of magic-angle bilayer graphene*, arXiv:1808.02482 (2018).
- [66] L. Fu and C. L. Kane, *Time reversal polarization and a z 2 adiabatic spin pump*, Phys. Rev. B **74**, 195312 (2006).
- [67] Accordingly, P_T here is gauge invariant modulo 1 while it depends on a gauge without C_{2z} symmetry. As P_T is quantized and gauge invariant in the presence of C_{2z} , it serves as a topological mirror invariant [69]. Notice that C_{2z} acts like a mirror on the time-reversal-invariant 1D subBrillouin zone.
- [68] Y. Choquet-Bruhat and C. M. de Witt, *Analysis, Manifolds, and Physics* (Gulf Professional Publishing, 1982).
- [69] A. Lau, J. van den Brink, and C. Ortix, *Topological mirror insulators in one dimension*, Phys. Rev. B **94**, 165164 (2016).